BACHELOR

Using statistical analysis on thermal time series for (non-)rotating Rayleigh-Bénard convection

van Helden, Sjoerd E.S.

Award date:
2018

Technische Universiteit Eindhoven University of Technology
Where innovation starts

Department of Applied Physics
Bachelor End Project

Using Statistical Analysis on Thermal Time Series for (non-)rotating Rayleigh-Bénard Convection

Sjoerd van Helden, 0893960
Jonathan S. Cheng, Matteo Madonia, Rudie P.J. Kunnen
Document number: R-1949-SE

Eindhoven, July 2018

Abstract

Temperature difference driven convection, commonly referred to as Rayleigh-Bénard convection, occurs in many different settings like the earth's atmosphere or its ocean's circulations. We investigate flow structures in (non-) rotating Rayleigh-Bénard convection experiments in water using thermal measurements. Any flaws of the experimental set-up are also looked into so that they can be dealt with for any future measurements. Fourier spectrum analysis and cross-correlations are used on thermal time series measurements in the top, bottom and side end walls. The Fourier spectra of the top end wall along with side end wall show strong influence of periodic cooling by the environment. This periodicity is related to the rotation rate which implies that the location of the source is not changing. The frequency of the cooling mechanism of the top plate is also found and this effect is dominant. The cross-correlations on this end wall confirm this, because short time scales are found along with strong positive correlation. The effect of heating on the bottom end wall is noticeable for the cross-correlations as well. Cross-correlations on the side wall indicate a Large Scale Circulation for non-rotational cases for high values of Rayleigh. This circulation consist of two rolls which are stacked on top of each other. For rotational cases a flow structure consisting of possibly four rolls, two on the upper half of the container and two on the bottom half are found. From the results it is theorized that the rolls on one side of the tank are compressed in the horizontal direction while the rolls on the other side are expanded in this direction.

Contents

1 Introduction **1**

2 Theory **2**
2.1 Time scales 2
2.2 Nu-Ra Scaling laws 3

3 Methods **5**
3.1 TROCONVEX 5
3.2 Acquisition of Data 5

4 Fourier Spectrum Analysis **9**
4.1 Fourier transform 9
4.2 Results and Discussion 11

5 Cross-correlations Analysis **15**
5.1 Analysis of the top and bottom plate 16
5.2 Analysis of the side walls 16

6 Conclusion **22**

A Time tables of the Top & Bottom plate **23**
A.1 Explanation of the tables 23
A.2 Time tables for the non-rotating cases 23
A.3 Time tables for the rotating cases 25

B Time tables of the Side walls **28**
B.1 Explanation of the tables 28
B.2 Time tables for the non-rotating cases 28
B.3 Time tables for the rotating cases 31

1 Introduction

One of the goals of this project is to gain more insight in flow structures generated via Rayleigh-Bénard Convection (RBC) that occur inside a cylindrical container. This container is filled with water, capable of rotating, and situated at the facility of WDY at Eindhoven University of Technology. This container is called the TROCONVEX and it is part of series of experimental set-ups used to gain a better understanding of RBC. The TROCONVEX will be described in more detail in chapter 3. Another goal is to find any flaws of the TROCONVEX that might affect the flow structures or the temperature measurements. Multiple thermistors are placed into the end walls of the TROCONVEX and these are used for temperature measurements. Time series analysis, Fourier spectrum analysis and Cross-Correlation analysis are used to extract useful information out of these measurements.

Turbulent convection is at the basis of natural, technological and astrophysical phenomena. A temperature difference is often the driving force behind these convections. This kind of convection is often referred to as Rayleigh-Bérnard Convection. On Earth the motion of air in the atmosphere, circulation in the ocean and its magnetic field can all driven by convection [1, 2, 3]. This kind of convection is also found at other planets and stars [3]. Convection is also the driving force behind the temperature regulation of buildings and cars and the manufacturing of electronic equipment [4, 5].

The most basic form of convection occurs via heating the bottom of a container holding some fluid while cooling the top. The fluid will then undergo RBC [6, 7]. The nature of this convection is depended on the properties of the fluid, the dimensions of the container, the temperature difference between the top and bottom and the power of the heating source. It is common to describe these properties as dimensionless parameters [8, 9]. The Rayleigh number $Ra = \gamma g \Delta T H^3/(\nu\kappa)$ describes the strength of upwards motion due to buoyancy compared to drag and gravity for some quantity of fluid. The quantity g stands for the gravity acceleration, γ for the thermal expansion coefficient and ΔT is the temperature difference between the top and bottom end wall. The Prandtl number $Pr = \nu/\kappa$ gives the ratio between the kinematic viscosity ν and the thermal diffusivity κ of the fluid. The aspect ratio $\Gamma = D/H$ gives the ratio between the diameter D and the height H of the tank.

For low values of Ra the fluid will be stratified in temperature. If the critical value for Ra is exceeded this state becomes unstable and so called cells of Rayleigh-Bérnard will start to occur as shown in figure 1. These cells transport hot fluid to the top via one side while simultaneously transporting cold fluid to the bottom via the other side. The amount of cells depends again on the parameters already mentioned [6, 7, 8]. This critical value for Ra is of order 10^3 and for most natural phenomena this critical value is exceeded. For example the estimated values for Ra in the Earth's outer core are of order $10^{20} - 10^{30}$ [10, 11]while current simulations can only reach values of Ra of order $\lesssim 10^7$ [12]. It is in these high regimes of Ra that knowledge is lacking, because current experiments and simulations cannot reach these regimes.

When the container in which RBC takes place is brought in rotation new phenomena occur [8, 13]. RBC in the rotating case is much less well understood than for the non-rotating case. A lot of research has been done on rotating RBC and the new regimes that occur. In order to describe the rotating RBC case and its regimes new dimensionless parameters need to be introduced. The first parameter is the Ekman number $E = \nu/(2\Omega H^2)$ which describes the relevance of the rotation rate Ω relative to ν [8, 13, 14]. The second parameter is the convective Rossby number $Ro = \sqrt{Ra/Pr}E$ which describes the relevance of Ω relative to the strength of vertical motion due to buoyancy [8, 13, 14]. The relationship between these parameters and the different regimes of non-rotating RBC are described in more detail in chapter 2.

In this report chapter 2 will give an overview of the necessary theory behind (non-)rotating RBC. Chapter 3 will explain the experimental set-up as well as the methods used to analyze the measured data. In chapter 4 and 5 the found results of Fourier spectrum analysis and Cross-correlation analysis will be discussed. These analyses are performed on thermal data from the side walls as well as the top and bottom plate. Chapter 6 will give a conclusion of the found results along with improvements for future experiments. Appendix A and B contain tables that include the full results of the Cross-correlation analysis

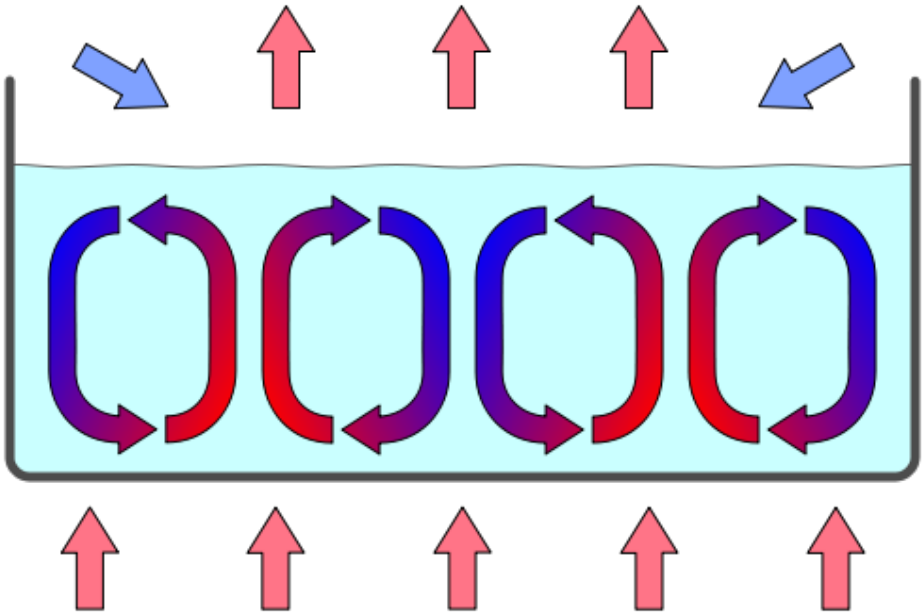

Figure 1: A schematic of RBC cells for a container with an open top. Heat enters the fluid from below and via the cells it is transported to the open top. The open top allows for the heat to then escape and cooling the fluid. [15]

2 Theory

2.1 Time scales

For rotating Rayleigh-Bérnard Convection multiple fundamental time scales can be defined which give a clearer relationship between the dimensionless parameters and the flow structures [16]. The buoyancy forcing (free-fall) time scale $\tau_{ff} = H/U_{ff}$ is defined as the ratio of the height of the tank and the free fall velocity $U_{ff} = \sqrt{\gamma g \Delta T H}$. The viscous diffusion time scale and the thermal diffusion time scale are defined as $\tau_\nu = H^2/\nu$ and $\tau_\kappa = H^2/\kappa$ respectively. The rotational timescale $\tau_\Omega = 1/(2\Omega)$ is simply the inverse of the rotation rate halved. Given these time scales an alternative way can be used to define the dimensionless parameters as follows:

$$Ra = (\tau_\nu \tau_\kappa)/\tau_{ff}, \quad Pr = \tau_\kappa/\tau_\nu, \quad E = \tau_\Omega/\tau_\nu, \quad Ro = \tau_\Omega/\tau_{ff}. \tag{1}$$

The parameters of equation (1) are equal to the parameters mentioned in chapter 1 if the time scales are filled in. However none of these parameters give an indication of how dominant convective heat transport in a given (non-)rotating RBC is. The dimensionless parameter that does do that is the Nusselt number $Nu = qH/(\kappa \rho C_p \Delta T)$, because Nu relates the total heat transfer with conductive heat transfer as a ratio between the two [16, 17]. Here ρ is the density of the fluid, C_p the specific heat capacity and q the heat flux per unit area.

Dynamo models also give time scales which are relevant for rotating RBC. The Reynolds number Re which relates the inertial forces to the viscous forces can be theorized by these models via scaling laws. The exact nature of these scaling laws is depended on some assumptions which are made in the model. The three scaling models that will be discussed are the *inertial scaling*(CIA), the *magneto-Archimedean-Coriolis balance*(MAC) and the *viscous scaling*(VAC) [12]. Because the length scale of the experiment is known and $Re \sim U$ a time scale for each scaling can be determined as follows:

$$t_{sc} = \frac{H^2}{Re_{sc}\,\nu}. \tag{2}$$

Here t_{sc} and Re_{sc} is the time scale for some scaling law. The Reynolds numbers for each scaling law is determined via the equations

$$Re_{CIA} \sim C^{2/5}E^{1/5}, Re_{MAC} \sim C^{1/2}E^{1/2}, Re_{VAC} \sim C^{1/2}E^{1/3} \tag{3}$$

where $C = Ra(Nu-1)/Pr^2$ is called the convective power for thermal convection [12]. The Re's of equation (3) can then be plugged in equation (2) so that the time scale for each scaling model can be determined. It should be noted that these Reynolds numbers are approximations, because it is assumed that each equation of (3) needs to be multiplied by some constant. The value of this constant is not yet known and is different for each scaling law. However these time scales still give a good indication of how large the actual time scales should be.

2.2 Nu-Ra Scaling laws

The Nusselt number is predicted to be depended on Ra, Pr and E, that is

$$Nu \sim Ra^{\alpha}Pr^{\beta}E^{\delta} \tag{4}$$

for both non-rotational and rotational RBC [16, 9, 18]. The exponents α,β and δ of equation (4) are constants and are different depending on the flow regime. The scaling theory of Malkus predicts a scaling law of $Nu \sim Ra^{1/3}$ [9, 19, 20]. The exponent of 1/3 is also found if it is assumed that the boundary layers at the top and bottom end wall of the container do not communicate. The scaling theory by Shraiman and Siggia assumes that near the boundary layer shear-flow turbulence exists and that results in a scaling law of $Nu \simeq 0.27Pr^{-1/7}Ra^{2/7}$ [9, 21, 20]. The Chicago mixing zone model describes a similar dependency except Pr scales with 2/7 instead [18]. Kraichnan derived for large values of Ra, commonly referred to as the ultimate regime, scaling laws of $Nu \sim (RaPr)^{1/2}$ for $Pr \leq 0.15$ and $Nu \sim Ra^{1/2}Pr^{-1/4}$ for $0.15 < Pr \leq 1$ [9, 22, 20]. Grossmann and Lohse described multiple different scaling theories depending on the values of Ra and Pr [18, 20]. For $Ra \leq 10^{11}$ they described a scaling law $Nu \sim Ra^{1/4}Pr^{1/8}$ for $Pr \lesssim 1$ and $Nu \sim Ra^{1/4}Pr^{-1/12}$ for $Pr \gtrsim 1$. For large values of Ra multiple scaling laws are derived. For medium values of Pr they describe a similar power law as Kraichnan and for large values of Pr they describe a power law similar to that of Malkus. For small values of Pr $Nu \sim Ra^{1/5}Pr^{1/5}$ and for very large values of Pr $Nu \sim Ra^{3/7}Pr^{-1/7}$.

For the rotating case Nu will scale with E again as a power law. For fixed values of E figure 2 shows the Nu dependency on Ra while also indicating the many rotating RBC regimes [16]. The *columnar regime* occurs at low values of Ra and Nu. In this regime heat is transported via convective Taylor columns [13, 16]. These columns extend across the whole bulk from boundary layer to boundary layer and therefore they dominate the heat transfer. Convective Taylor columns are generated by plumes which stay attached to the boundary layer. The column's inner core is protected by an outer surface of oppositely-signed vorticity. Convective Taylor columns are not found for $Pr < 3$, for these values of Pr plumes dominate the heat transfer instead [13, 16]. For larger values of Ra these columns start to break apart in the vertical direction leading to the creation of plumes (*the plumes regime*). The plumes generated at the boundary layers can no longer stick to them and instead move away from them. These plumes have a similar length scale as the convective Taylor columns, but they no longer extend across the entire length of the container. For even larger values of Ra the plumes stick closer to the boundary layers and the bulk of the fluid becomes a well-mixed turbulent layer created by vortex-vortex interactions [13, 16]. This regime is often referred to as the *geostrophic turbulence regime*. For very large values of Ra the *unbalanced boundary regime* is reached, but not a lot is known about this regime. However it is estimated that the thermal boundary layers break down. For huge values of Ra the flow field becomes insensitve to the Coriolis forces and the bulk becomes nearly isothermal. The temperature difference is completely confined to the boundary layers. This last regime is not reached by the TROCONVEX.

The values for transitional Rayleigh numbers are still somewhat unclear. Predictions have been made relating these Rayleigh numbers to values of Ekman, but more research is needed. The transitional Rayleigh number from the columnar regime to the plumes regime is estimated to be $Ra_{CP} \sim 5.4E^{-1.47}$ for $Pr \approx 7$ [23]. For the transitional Rayleigh number from the plumes regime to the geostrophic regime no specific predictions exist [16].

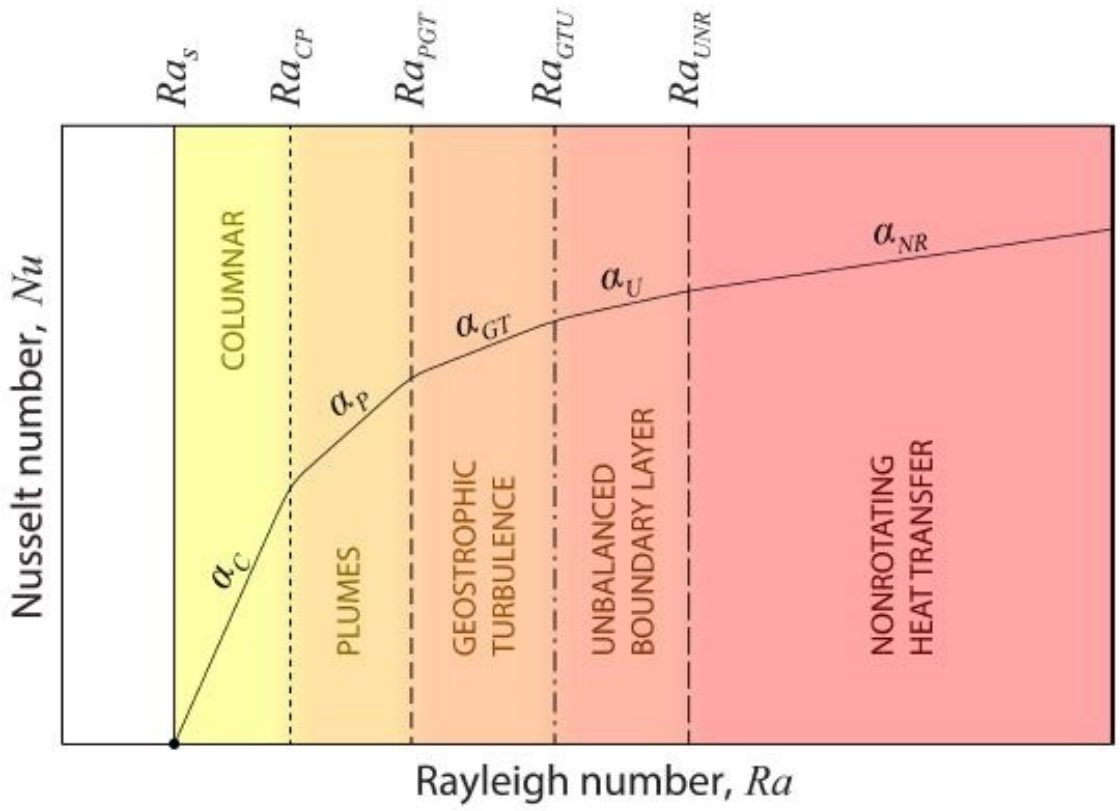

Figure 2: This schematic shows the distribution the regimes in terms of Nu versus Ra for $Pr > 3$. The vertical lines indicate transition Rayleigh values: Ra_s denotes convective onset, Ra_{CP} denotes the transition between columnar-style convection and plumes, Ra_{PGT} between plumes and geostrophic turbulence, Ra_{GTU} between geostrophic turbulence and unbalanced boundary layers, and Ra_{UNR} to nonrotating-style convection. [16]

Large Scale Circulations (LSC) which are generated in the container could also affect the Nu-Ra scaling [9, 20]. An LSC is generated via plumes of similar heat which cluster together which then give rise to a large-scale flow. The exact shape of an LSC is determined by the aspect ratio and the form of the container in which the LSC is generated. For aspect ratios equal to about 1 only one roll is expected while for aspect ratios greater or smaller than 1 two or more rolls can be present. If multiple rolls are present they could either lay on top of each other or next to each other and this orientation is constantly changing. Figure 3 shows two possible LSC's for tanks of $\Gamma < 1$. It can also not be excluded that smaller rolls get trapped in certain areas of a container which could also affect the *Nu-Ra* scaling. For higher values of *Ra* the influence of a LSC on Nusselt decreases. Non-Boussinesq effect could also cause results to be different then theorized. Theory assumes that the flow behaves Boussinesq i.e. that its properties do not change for different temperatures [16]. However for the more extreme regimes this assumptions does not have to be true.

3 Methods

3.1 TROCONVEX

The data used in this report is acquired from measurements made inside of the TROCONVEX. Figure 4 shows a side view schematic of the TROCONVEX. The TROCONVEX is a cylindrical tank of 2 m high and with a diameter of 0.4 m. The tank is capable of rotating up to $\Omega_{max} = 2.2$ rad s^{-1}, but has a minimum of $\Omega_{min} = 0.15$ rad s^{-1}. It is filled with water and heated at the bottom and cooled at the top. The bottom plate of the TROCONVEX has been isolated so that all the heat generated by the heating element located under this plate is all directed into the tank. The top plate is cooled via a chiller which has two ways cooling. The first method is via indirect cooling, the cooling water from the chiller is first heated in a heat bath before this water is used to cool the top plate. This is done to prevent too strong cooling for when the bottom is heated for small values of q and to keep thermal amplitude changes in the top plate small. The second method is via direct cooling, the heat bath is no longer used and the top plate is directly cooled via the chiller. This method is only used when the bottom plate is strongly heated. The top plate is not as well isolated as the bottom plate. The cylindrical side wall is actively isolated by measuring the heat flux and then using heating elements on the sides to neutralise it. The temperature difference ΔT that the TROCONVEX is capable of ranges from 1 up to 25 degrees Celsius.

On two opposite sides of the cylindrical side wall (indicated as side A and side B) 5 thermistors on each side have been installed. They are numbered 1 through 5 (for each side) where thermistor 1 is closest to the bottom and thermistor 5 is closest to the top. Thermistor 3 is located exactly at 1 m, half of the total height of the tank. No difference exists between side A or B so that the heights of the thermistors at A are equal to the heights at B. Figure 4 shows the exact distances between the thermistors and the plates via coloured arrows, green being equal to 0.4 m while purple is 0.2 m. It should be noted that these arrows are not drawn to scale.

Eight thermistors are placed in both in the top and bottom plate. They are positioned in a cross where the lines of the cross are diagonals and a ninety degree angle is made between these two lines. The thermistors are spaced equally between each other as can be seen in figure 5 for both the top and bottom plate. The picture on the left is the top plate and the picture on the right is the bottom plate. One thermistor of the top plate is broken and its data is not used. The orientation of the top plate's thermistors with respect to either side A, side B or the bottom plate is not known and this is also true for the bottom plate. This means that specifically cross-correlations between either plates with either each other or one of the side walls will not give verifiable results. The time lags obtained via cross-correlations have no meaning without knowing the distances between the two thermistors of which the correlation is taken.

3.2 Acquisition of Data

In total there are thirteen different cases that are analyzed and table 1 gives the relevant parameters. The cases are compared with each other to see which give reasonable results and which cases should be excluded. The dimensionless parameters of column 4 through 7 of table 1 are calculated using properties of the fluid, the tank and thermal data. From this point forward the case number will only be given whenever an analysis

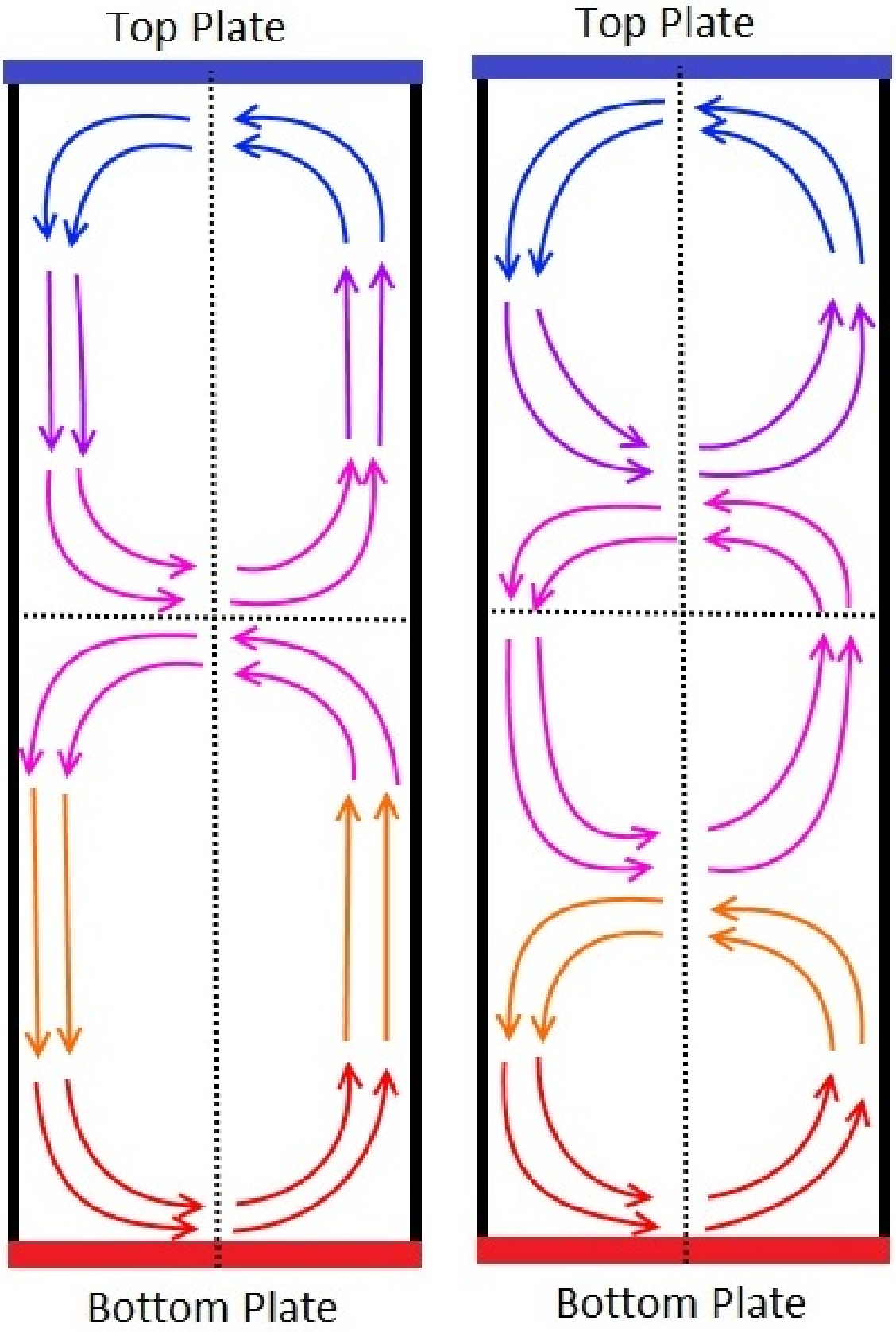

(a) *(b)*

Figure 3: Two skethes of possible LSC configurations are shown for $\Gamma < 1$. The sketch on the left shows 2 rolls stacked on top of each other while the sketch on the right shows 3 rolls. The colour of the arrows gives an indication of the local temperature and the direction of the arrows the direction of flow.

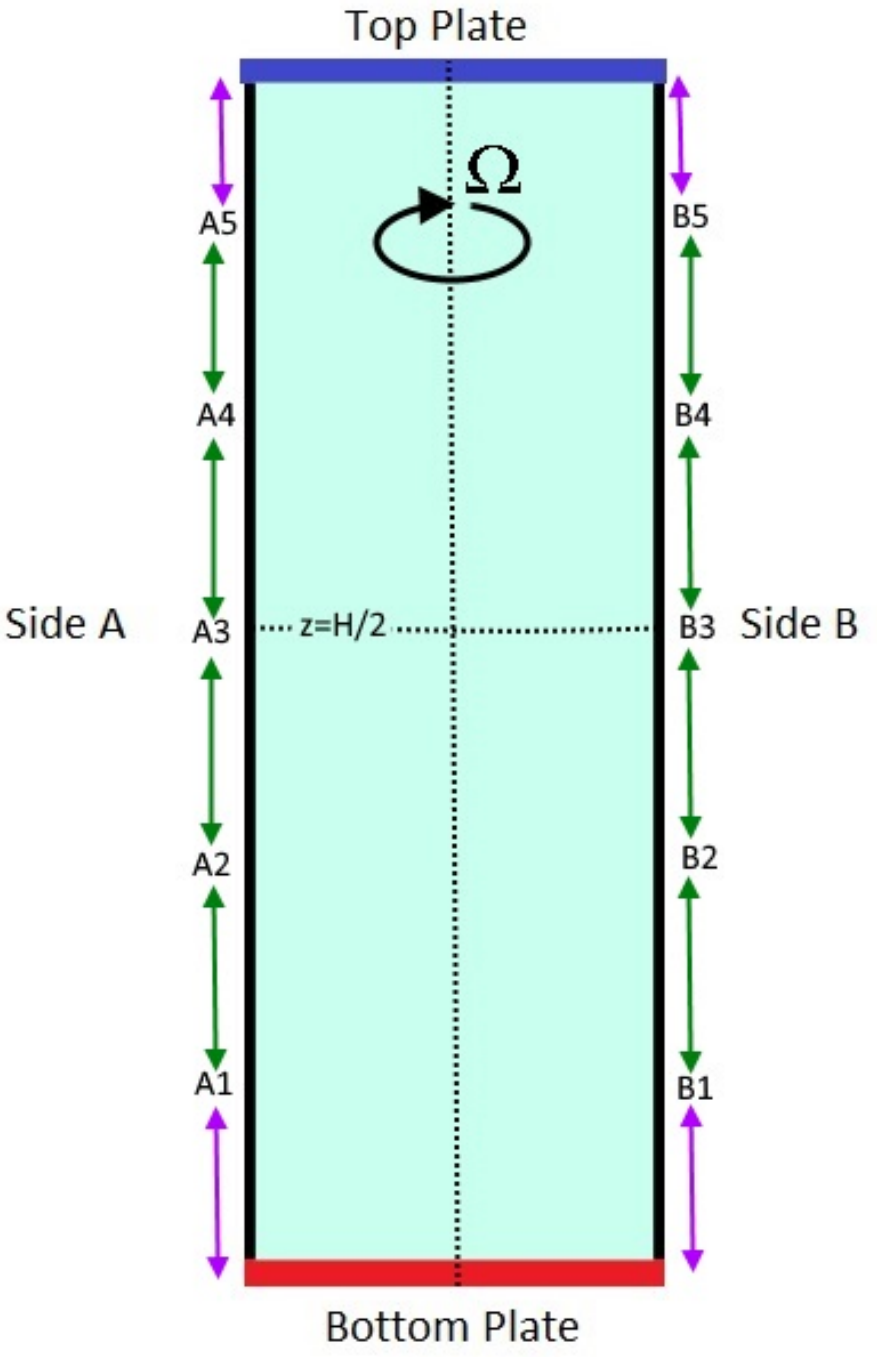

Figure 4: A schematic of the TROCONVEX is given and not to scale. The Bottom plate is heated from below while the top plate is cooled so that ΔT stays constant during the measurement. The thermistors inside these plates are not shown here. However the side wall thermistors are and are indicated as either A1-A5 or B1-B5. Thermistors A3 and B3 are located at the vertical halfway point. The vertical dotted line shows the axis of rotation along with the centres of both the plates. The green arrows indicate a distance of 0.4 m between two thermistors while the purple arrows indicate a distance of 0.2 m between a thermistor and a plate. The direction of rotation and the sides A and B are arbitrary for the orientation is cylindrically symmetrical.

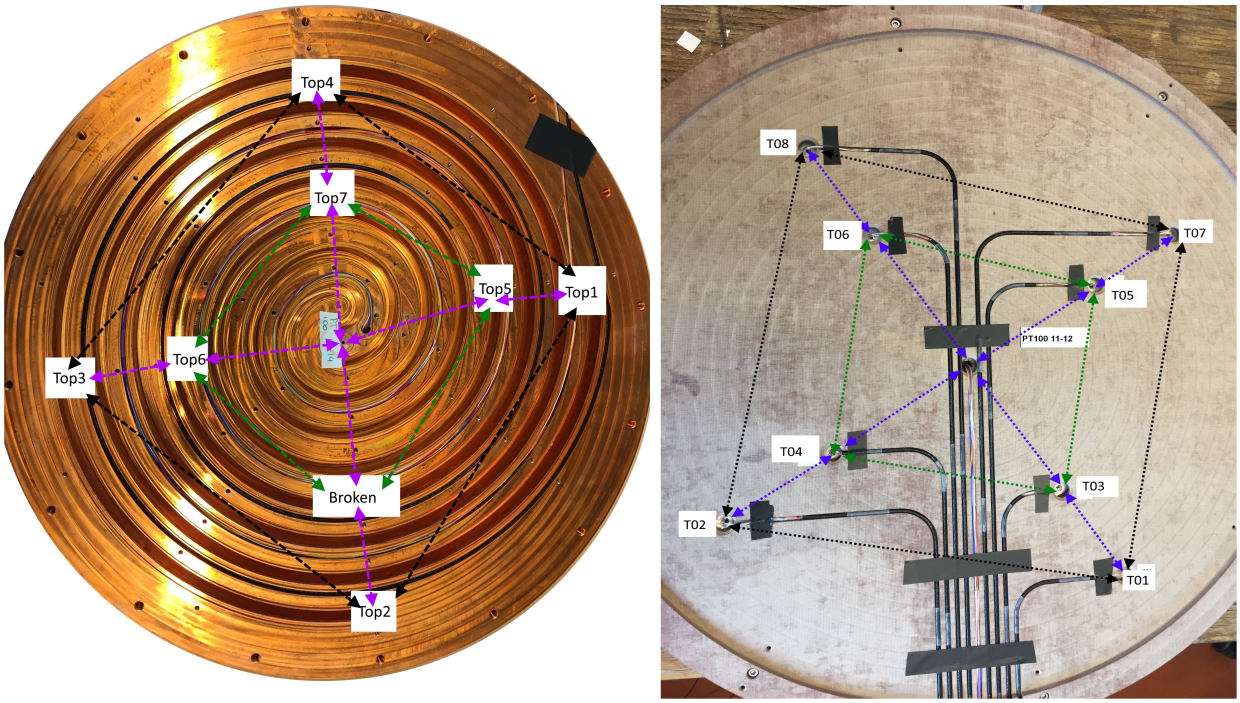

Figure 5: ***Left****: A picture of the top plate is shown along with the location of the thermistors. The broken thermistor is also shown here. The loop through which the cooling water flows can be seen here and has a spiral shape. The tube first spirals inward and then it spirals outward again so that the water can leave the surface of the top plate.* ***Right****: A picture of the bottom plate is shown along with the location of the thermistors. For both pictures the colour of the arrows indicate the distance between 2 thermistors: a purple arrow indicates a length of 66.7 mm, green a length of 94.2 mm and black a length 189 mm. Arrows of the same colour can differ in length in this figure, because the perspective of the picture warps the locations of the thermistors somewhat. The white boxes obscure the exact location of the thermistors which influences the length of the arrows as well. However for the bottom plate it is not as bad as with the top plate.*

is performed. To verify the validity of the TROCONVEX its *Nu-Ra* dependency is compared to that of other studies and the theory. Figure 6 shows the dependency of the Nusselt on Rayleigh. In this figure it is clearly observed that for larger Ra Nu also rises, but for very large Ra the graph flattens just like the theory shows. Figure 2 shows the theoretical behaviour of Nu vs Ra and this graph is similarly shaped as figure 6 which is promising. Similar graphs and dependencies are found by other researchers [24].

Table 1: This table gives the relevant parameters of all cases that are examined. The first column gives the case number, the second column gives the power setting of the heating element in Watts, the third column gives the angular velocity of the tank in rotations per minute and column 4 through 7 gives the dimensionless parameters. For all cases $\Gamma = 1/5$*. For case 8 the Ekman number is an estimate based the results from the other 3 RPM cases. This is done because no Ekman number was calculated for this case. However given the consistency of E for the 3 RPM cases this is a reasonable estimate.*

Case	Q (W)	Ω (RPM)	Ra	Pr	E	Nu
1	10	0	1.9E+11	5.21	∞	315.92
2	20	0	3.4E+11	5.21	∞	344.13
3	50	0	6.6E+11	5.21	∞	453.29
4	100	0	1.1E+12	5.21	∞	537.33
5	200	0	1.9E+12	5.18	∞	645.04
6	500	0	3.8E+12	5.21	∞	782.39
7	1000	0	6.5E+12	5.22	∞	921.09
8	10	3	1.9E+11	5.22	3.00E-07	308.36
9	50	3	3.3E+11	5.25	3.00E-07	356.14
10	100	3	1.1E+12	5.26	3.00E-07	510.79
11	500	3	3.9E+12	5.23	2.99E-07	756.98
12	1000	3	6.5E+12	5.21	2.98E-07	908.25
13	200	18	2.5E+12	5.20	5.00E-08	488.50

The thermal data of the thermistors is acquired by heating the bottom plate and keeping ΔT constant for the entire measurement. This means that the temperature of the top plate is directly controlled to meet this condition. The measurement takes place over multiple hours so that the flow can develop properly. The temporal data is then sent to a computer and saved there. No significant differences exist between measuring for rotating or non-rotating cases. Afterwards the time series of the temporal is checked so that it can be truncated. This is done because the first couple of hours of a measurement are not useful, because the flow has not fully developed yet. This initial phase can easily be spotted, because the temperature of each thermistor is rising with similar speed. This truncated data is then used for different kinds of analysis. Chapter 4 and 5 describe how the data is actually used. Standard software for Fourier spectrum analysis and cross-correlation analysis is used.

4 Fourier Spectrum Analysis

4.1 Fourier transform

The Fourier transform is a tool that transforms a waveform or signal into a sum of sine and cosine functions [27, 28, 29, 30]. These functions could be considered the building blocks of the signal. The main advantage of performing this transform is that sinusoids are well understood functions and these functions have two clear parameters: an amplitude and a frequency. In most cases a signal will consist out of multiple of these sinusoids and therefore multiple amplitudes and frequencies are acquired. These parameters therefore function as a "fingerprint" of the signal and this fingerprint can be further analyzed to conclude if it holds any valuable information. Some frequencies could be related to timescales and flow structures and some frequencies are related to environmental and experimental causes. The amplitude that accompanies a certain frequency gives the importances of this frequency with regard to the original: the larger the amplitude, the more dominant the accompanying frequency.

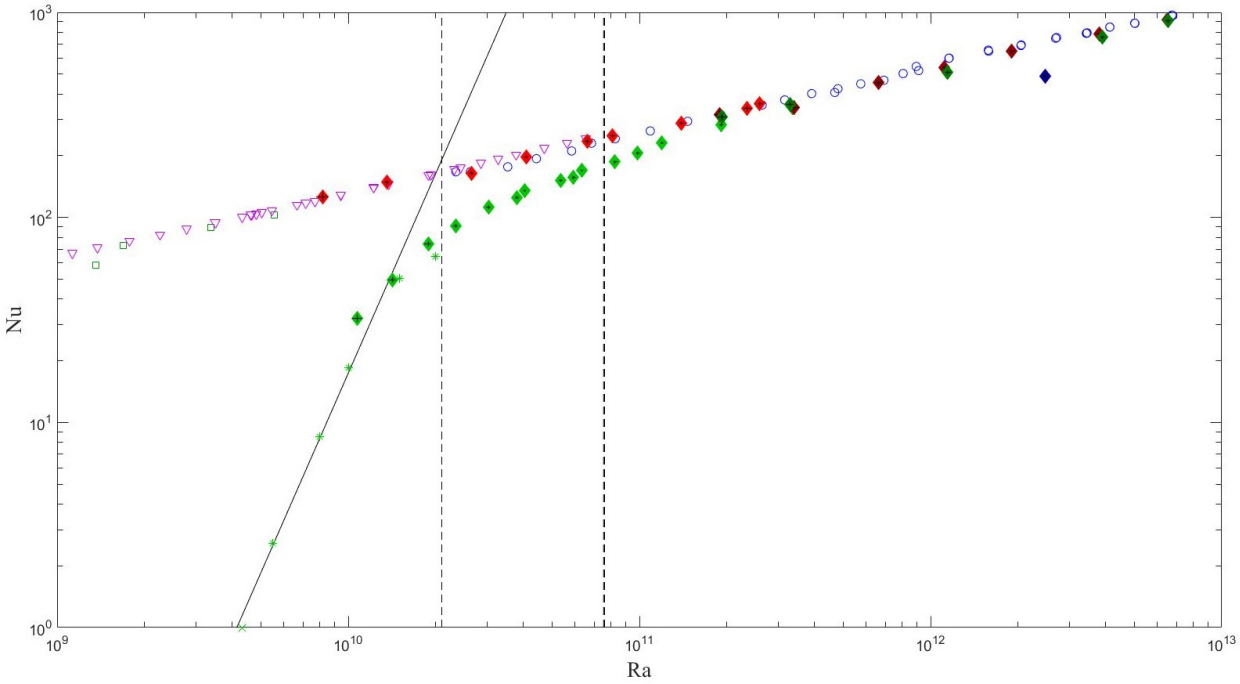

Figure 6: This graph shows the dependency of Nu on Ra. The shape of the graph is in perfect agreement with the theory and former research. The data points that are not filled in are taken from other experimental setups while the coloured data points are taken from data of the TROCONVEX. The purple triangles is data taken from Ahlers et al. (2006) [25], the green squares is data taken from King et al. (2012) [26] and the blue circles is data taken from Cheng et al. (2015) [23]. The green stars are preliminary data point from a different experimental setup in Eindhoven University of Technology. The red diamonds represents data from the TROCONVEX for $\Gamma = 1/2$ while the green diamonds represents data for $\Gamma = 1/5$. The darker shade for some of the diamonds means that this data was taken from cases where $\Omega > 0$ RPM. The blue diamond is for the case where $\Omega = 18$ RPM.

Let $g(t)$ be some function depending on time t and let $\mathscr{F}$ be the Fourier transform function then the Fourier transform of $g(t)$, $G(f)$, is given by

$$\mathscr{F}\{g(t)\} = G(f) = C\int_{-\infty}^{\infty} g(t)\exp^{-2i\pi ft}\,dt \tag{5}$$

where f is the frequency and C is a normalization constant which commonly is set to $1/(2\pi)$ [27, 28]. One of the beautiful properties of the Fourier transform is that it is symmetrical. If $g(t)$ and $G(f)$ are swapped in equation (5), the minus is replaced by a plus in the exponent and the integral is taken over the frequency domain instead i.e. dt is replaced by df the Inverse Fourier transform is obtained. This means that the original function $g(t)$ can be obtained from its own Fourier transform $G(f)$. However equation (5) or its inverse cannot be used on data sets or signals, because these sets and signals are not continuous but discreet. Therefore instead the Discrete Fourier Transform(DFT) is used. Software programs often use an algorithm called the Fast Fourier Transform(FFT) instead, because it takes less computation time to perform. The FFT is used so often to calculate the DFT that the terms FFT and DFT are used interchangeably by people. The DFT is defined as follows:

$$G(k) = \sum_{n=0}^{N-1} g(n)\exp^{\frac{-2i\pi kn}{N}} \tag{6}$$

where N is the total number of samples, n the sample number and k the dimensionless frequency [29, 30]. Equation (6) differs only from equation (5) in that the integral is replaced by a summation. Note that k is dimensionless and the sampling frequency F_s is needed to convert k into a real frequency. The sampling frequency can be acquired by taking the inverse of the sampling rate T_s. For *all* data sets in this report $F_s = 1\,\mathrm{s}^{-1}$.

4.2 Results and Discussion

First Fourier spectra are taken for the top and bottom plate for all cases. For the low wattage cases the spectra for the top plate shows a bump at $f_{bump} \approx 1$ mHz as can be seen in figure 7. For higher wattage this bump disappears, but changing Ω has no effect on the bumps. The bump is never present at the bottom plate or at any of the side walls. Therefore, it is likely that these bumps are caused by the first method of cooling from the chiller. This cooling process has a frequency $f_{chiller} = 1/900 = 1.11$ mHz and this corresponds well with the bumps that are found.

There are also peaks located at higher frequencies, but only in the top plate and in side wall thermistors A2, A3 and B3. These peaks are only present for these thermistors if the rotation rate is nonzero. These peaks are also found at the thermistor that measures the room temperature (room thermistor). This thermistor is attached to the TROCONVEX, but it is not in contact with the fluid in any way. Figures 8 and 9 show the power spectra of multiple thermistors in the top and bottom plate along with the room thermistor spectrum in yellow. Subfigures 8c and 8d show that the bottom plate thermistors do not have this peak. Subfigures 8b, 9a and 9b show clearly that these peaks found at the room thermistor are the same as the other peaks for some of the top plate thermistors. The location of the top plate thermistors does not affect the likelihood of the appearance of these peaks. The frequency of this *room temperature peak* $f_{room} = 51.4$ mHz ≈ 3 RPM which suggests that $f_{room} \approx \Omega$. That would explain why this peak is not found for non-rotating cases. In order to confirm this hypothesis the Fourier spectrum of case 13 (the only 18 RPM case) is taken and for this case $f_{room} \approx 18$ RPM. Figure 10 shows multiple peaks, but the largest one is located at $f_{room} = 303$ mHz ≈ 18 RPM confirming the hypothesis. The cause for the other peaks seen in figure 10 is less clear. However they are equally spaced with gaps of sizes ~ 40 mHz which gives the impression that these peaks are not caused by a physical effect, but instead is a flaw of the thermistors itself.

It is reasonable to state that the frequencies f_{room} are not flow related, but instead are caused by the environment in which the TROCONVEX stands. Improving the isolation of the thermistors that are affected and/or removing the source of the problem is advisable. Especially for the three side wall thermistors improving the isolation is advisable, because these thermistors have this peak for all cases unlike the top plate thermistors where the affected thermistors change per case. It is also not sure how much improving

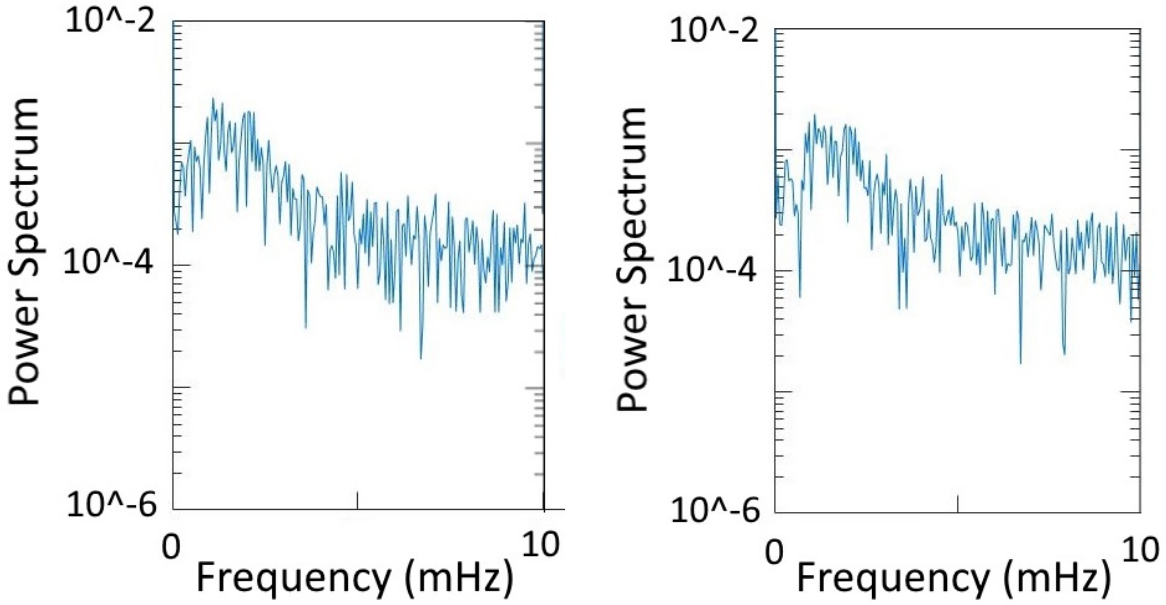

Figure 7: Fourier spectra of two different thermistors of the top plate for case 2. The bump around $f \approx 1$ mHz corresponds with the frequency of which the chiller cools the top plate. These bumps are not found in the bottom plate or side wall thermistors as well as for the top plate thermistors if Q is large. The rotation rate has no effect on this bump.

the isolation of the top plate will help with gaining better measurements and results, because the bottom plate, which is well isolated, has not given any interesting frequencies that could give an insight into the flow structures. The top plate has the added issue of the chiller affecting its measurements reducing the chance of seeing improvements in the data after the plate has been better isolated. An alternative to improving the isolation of the top plate is to use a multiband filter which is capable of filtering out the unwanted frequencies, $f_{chiller}$ and f_{room}. The fact that no peaks are found for the bottom plate thermistors gives an indication that the boundary likely does not vary in temperature, but instead is homogeneous.

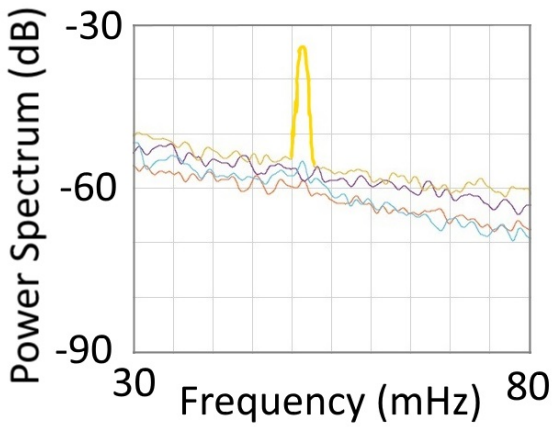

(a) A graph of the Fourier spectrum for the even thermistors of the top plate. These thermistors do not show the room temperature peak.

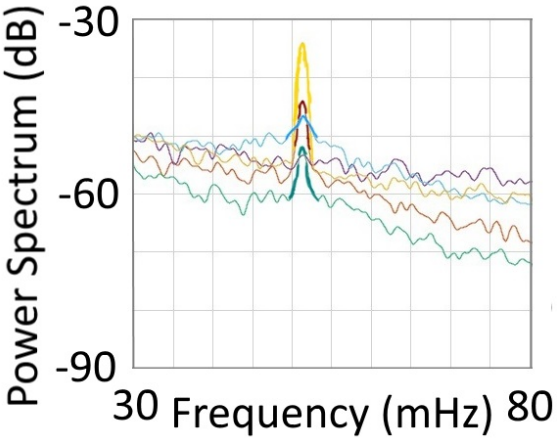

(b) A graph of the Fourier spectrum for the odd thermistors of the top plate. Some of these thermistors show the room temperature peak

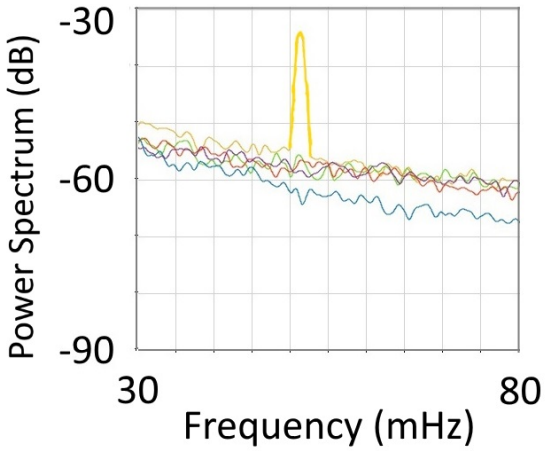

(c) A graph of the Fourier spectrum for the even thermistors of the bottom plate. These thermistors do not show the room temperature peak.

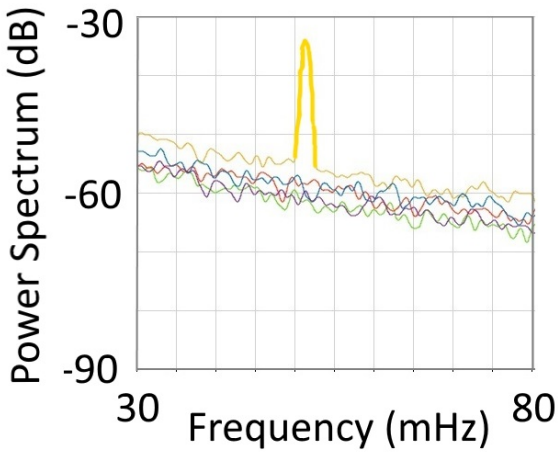

(d) A graph of the Fourier spectrum for the odd thermistors of the bottom plate. These thermistors do not show the room temperature peak

Figure 8: Graphs of the Fourier spectra for case 11. The yellow line indicates the Fourier spectrum of the thermistor that measures the room temperature. These spectra are comparable with the results for other 3 RPM cases. However the thermistors that show this peak do change per case.

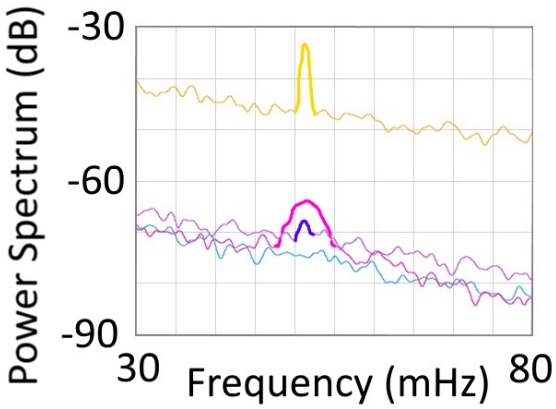

(a) A graph of the Fourier spectrum for the even thermistors of the top plate. A peak is found here for two of the thermistors compared to no peaks found in subfigure 8a.

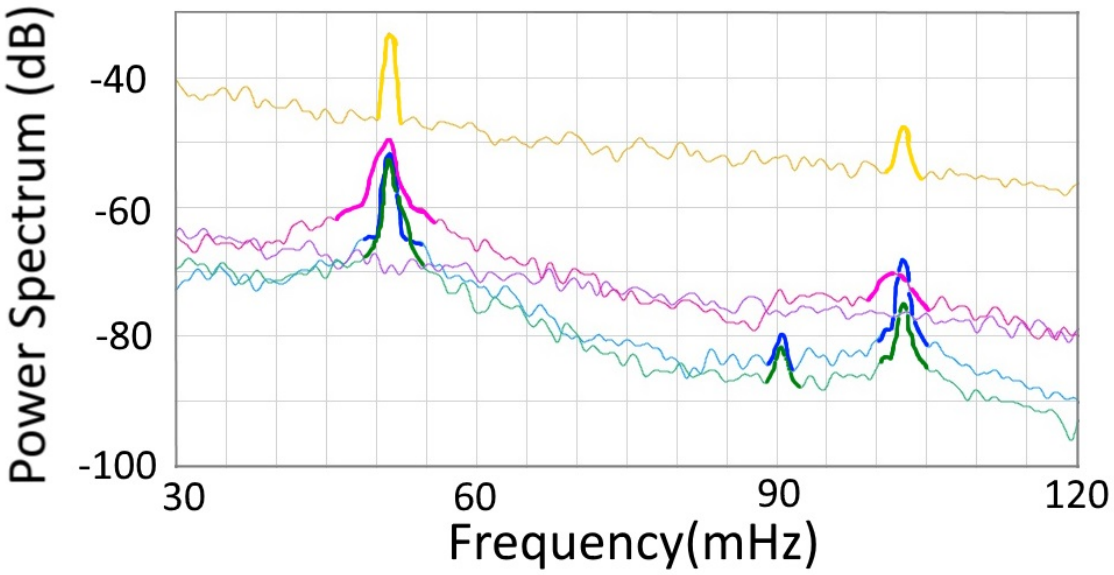

(b) A graph of the Fourier spectrum for the odd thermistors of the bottom plate. These thermistors do show the room temperature peak as well as the harmonics. The peaks at around 90.4 mHz are likely not flow related either. These peaks do not show up for other cases or thermistors which makes these peaks odd. For higher frequencies an artificial periodic disturbance is observed and that is likely the culprit of these 90.4 mHz peaks.

Figure 9: Graphs of the Fourier spectra for the top plate for case 10. The yellow line indicates the Fourier spectrum of the thermistor that measures the room temperature. These spectra look similar to that of figure 8. The spectra of the bottom plate are not included here, but look similar to that of figure 8

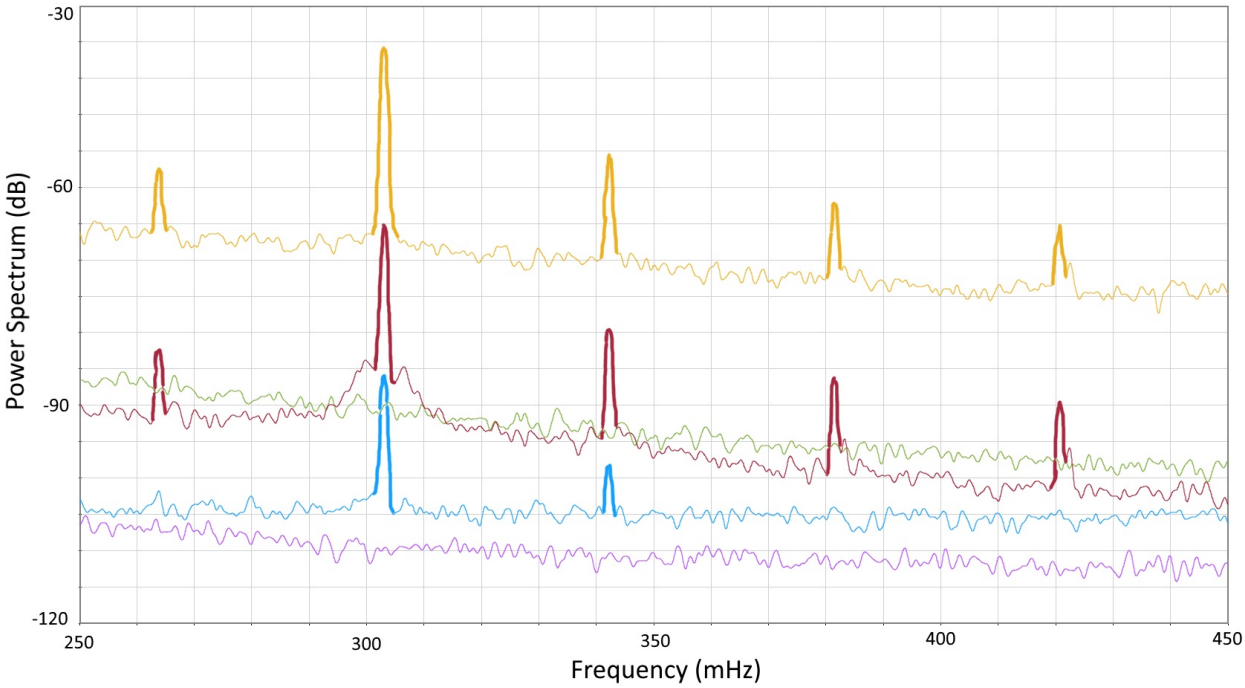

Figure 10: A graph of the Fourier spectrum for the even thermistors of the top plate for case 13. A peak is found here for two of the thermistors compared to no peaks found in.

5 Cross-correlations Analysis

Cross-correlations is another method that is used to gain more insight into flow structures as well as finding flaws of the experimental setup. The cross-correlation function measures the dependance between two signals. For sampled signals the equation is defined as

$$C_{ba} = \frac{1}{N} \sum_{n=1}^{N-m+1} b(n)a(n+m-1) \tag{7}$$

with $m = 1, 2, 3, \ldots, N+1$, N is equal to the total number of samples and a and b are time series of two different thermistors [31]. Both a and b are normalized before their cross-correlation is taken. The Matlab function xcorr was used to perform cross correlations. This function approximates equation (7) instead of calculating it exactly which allows for faster computation without a significant loss in accuracy.

Cross-correlations are taken between time series of the different top thermistors, between time series of the different bottom thermistors and between time series of the different side thermistor with each other. For the side thermistors the amount of executed cross correlations is reduced to only its nearest neighbours. The nearest neighbours of a thermistor is defined as follows: The thermistor on the opposite side with the same index and the thermistors located on the same side with a differing index of 1. No cross correlations were done between time series of the top and bottom end walls, because the locations of the top thermistors relative to the bottom thermistors is not known. For the same reason no cross correlations were done between any of the side end walls and either the top or bottom end wall.

A cross correlation between two different thermistors will give two results: A time lag and the strength of this correlation. The time lag can be compared with multiple relevant timescales to get a better understanding of the flow structures within. The time lag can also give the direction of the flow. A negative time lag indicates a flow that moves from the thermistor with a higher index to a thermistor with a lower index. A positive time lag indicates a flow moving in the opposite direction.

The strength of the correlation indicates the relevance of the associated time lag. A weak correlation indicates that the associated time lag should be ignored while a strong correlation indicates that the time lag is possibly valid. The strength of the correlation is normalized so that the autocorrelation at a time lag of 0 is defined

as 1 [8, 31]. The strength of a correlation then ranges between -1 and 1. A strong anticorrelation is also of interest, because that could indicate a temperature rise at one thermistor while the temperature at another thermistor is dropping. The maximum time lag has been set to 3600 seconds (1 hour). Any time lag that is higher will very likely not be physical, because the theoretical values for time scales are much lower.

5.1 Analysis of the top and bottom plate

For the bottom end wall strong positive correlations were found along with time lags of $\pm$ 60 s or less for the 3 rpm cases. Tables with all the time lags and correlation strengths are located in appendix A. For the 0 rpm cases the strength of the correlations becomes weaker as can be seen in figure 11. However for thermistor pairs where a correlation is found the time lags are of a similar order of magnitude. Raising Nu and Ra seems to have no effect on the time lags for the non-rotating cases. Both the direction of the flow and its timescale changes for different values for Nu and Ra, but not consistently. This can probably be attributed to the fact that the thermistors are located inside the bottom plate and are therefore always consistently heated by the heating element below. This would explain the strong correlation that is found and the inconsistency of the time measurements, because the thermal data of the thermistors is affected by the temperature of the heating element. The effects that boundary layers on the bottom plate potentially cause should also not be excluded, but more insight is needed about the exact nature of these boundary layers first. It can be excluded that any outside influences are causing these inconsistencies, because the bottom end wall is well isolated and Fourier spectrum analysis does not show anything that would be expected if outside influences were relevant. It would be fruitful to perform a similar analysis for the 0.8 m tank to see if similar correlations and lags are found there as well. Case 13 gives similar results as for the 3 rpm cases, but the time lags are much larger. The 2-minute mark is easily surpassed for some thermistor pairs. Because there is only one measurement in this rpm range no conclusions about the time lags' consistency or accuracy can be concluded.

The top end wall has compared to the bottom a weaker correlation and the time lags are shorter as well. There seems to be no noticeable difference between either the rotating or non-rotating cases which is unexpected as can be seen in figure 11 and figure 12. Raising Nu and Ra also does not seem to affect the time lags either. The inconsistency that was found at the bottom plate is found here as well, but likely the source of this inconsistency is different. The top plate, unlike the bottom plate, is not well isolated and is therefore more vulnerable to outside influences. This is confirmed by the Fourier spectrum analysis, because significant peaks are found that correspond with the room temperature thermistor. These unwanted frequencies are likely the cause, because figure 11 and figure 12 shows strong periodicity. Similar to the bottom end wall the thermistors in the top are also embedded into the plate which could affect measurements. Potential effects caused by boundary layers cannot be excluded either, but more insight is needed about these boundary layers here as well. Another effect that could explain the relative short time lags in the top plate is that the top plate is cooled via the chiller as mentioned in chapter 3. Cold water from the chiller flows quickly over the top plate and this cooling could be measurable. Fourier spectrum analysis has already identified the cooling by the chiller(see chapter 4). The changing cooling method could explain the anticorrelation that is found for the high wattage cases.

5.2 Analysis of the side walls

First the side wall thermistors that are located at opposite sides of the TROCONVEX, but at the same height are analyzed. Appendix B holds all the tables which contain the correlation strength and time lags found for each case. For non-rotating cases and for low to medium wattages no correlation between these thermistors is found. For 1000W case strong anticorrelation was found between the thermistors closest to the plates. The found time scales are short and imply a flow of opposite direction. For the 500W case strong anticorrelation was found for all thermistor pairs except for A4-B4. For pairs 1 and 2 large time scales were found and the lags are in opposite direction. Pair 3 gives a short negative time scale while pair 5 gives a short positve time scale. For all 3 rpm cases anticorrelations are found between the middle three thermistor pairs. The time scale for pair 3 is negative and moves from ~ -40 s to ~ 0 s for increasing power. Pair 4 does the same except it moves from ~ 0 s to ~ 25 s. Pair 2 is not as well correlated as the other, but it seems like its time scale drops from ~ 80 s to ~ 50 s. Pair 2 and 4 do not behave like the theoretical time scales while pair 3 does. Possibly a reason for the strange behaviour of the time scales found for both rotating and non-rotating cases is that there is no direct flow between these pairs, but instead there is a general flow in

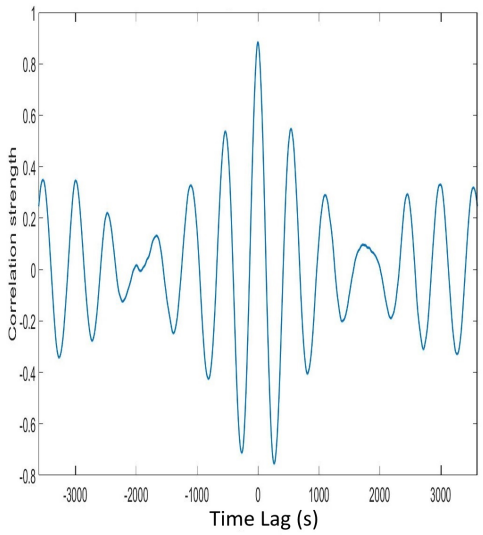

(a) This figure shows a lag vs. correlation plot for the thermistors 1 and 2 of the Top plate. Figure 5 shows the location of these two thermistors. Strong correlation is found, but the graph has multiple dominant peaks which indicates a weak correlation.

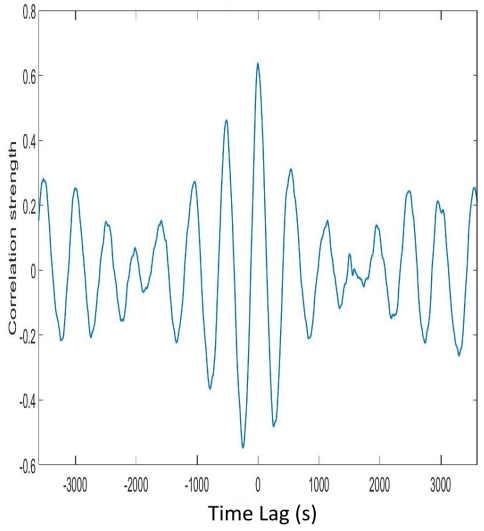

(b) This figure shows a lag vs. correlation plot for the thermistors 3 and 4 of the Top plate. Figure 5 shows the location of these two thermistors. Strong correlation is found, but the graph has multiple dominant peaks which indicates a weak correlation.

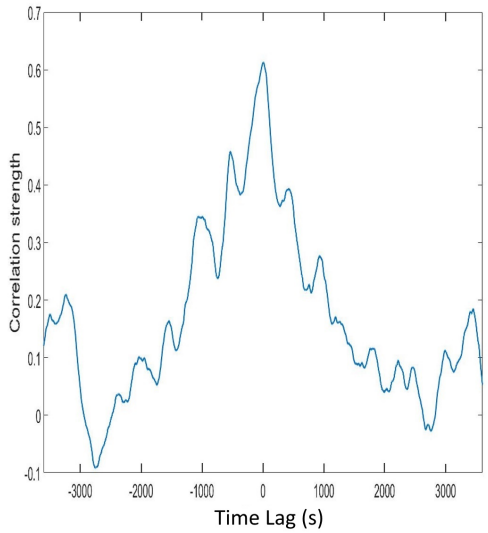

(c) This figure shows a lag vs. correlation plot for the thermistors 1 and 2 of the Bottom plate. Figure 5 shows the location of these two thermistors. There is a strong dominant peak at $t = -2$ s, but there are also weaker peaks around this peak. This indicates a weak cross-correlation. Weak correlations like this are observed for other non-rotating cases as well. The time lags that result out of those correlations are similar to this one.

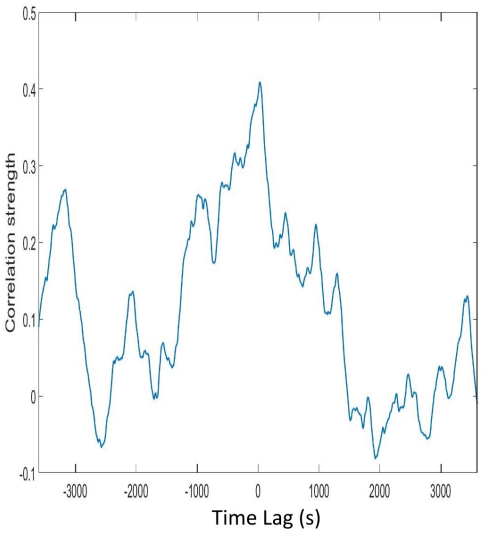

(d) This figure shows a lag vs. correlation plot for the thermistors 3 and 4 of the Bottom plate. Figure 5 shows the location of these two thermistors. There is a weak dominant peak at $t \approx 0$ s, but there are also weaker peaks around this peak. There is another dominant peak found at $t \approx 3100$ s. This indicates no correlations and this is also observed for other non-rotating cases.

Figure 11: Multiple graphs are shown which give the time lag vs. correlation strength of multiple thermistor pairs for the bottom and top plate. Graph a and b are graphs of the top plate and c and d are graphs of the bottom plate. These graphs are taken for case 5, however these graphs are representative for other non-rotating cases.

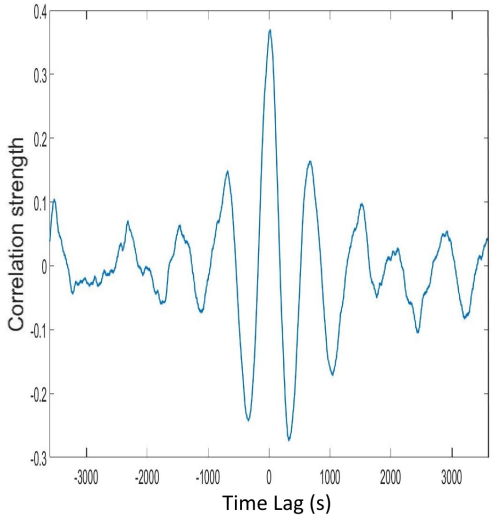

(a) This figure shows a lag vs. correlation plot for the thermistors 1 and 4 of the Top plate. Figure 5 shows the location of these two thermistors. Strong correlation is found, but the graph has multiple dominant peaks which indicates a weak correlation.This graph has a similar shape as figure 11a and 11b.

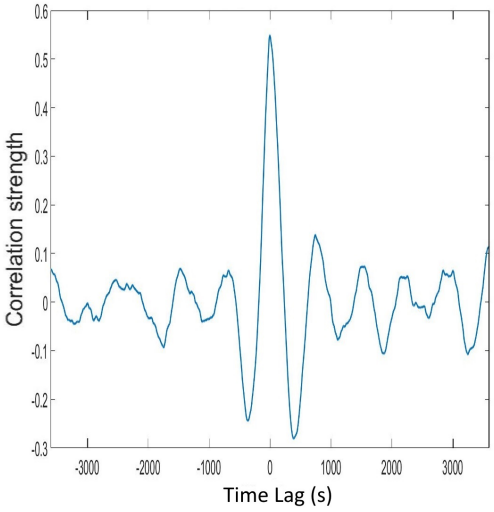

(b) This figure shows a lag vs. correlation plot for the thermistors 3 and 6 of the Top plate. Figure 5 shows the location of these two thermistors Strong correlation is found, but the graph has multiple other peaks, but none of them are dominant enough. This graph is associated with a strong correlation.

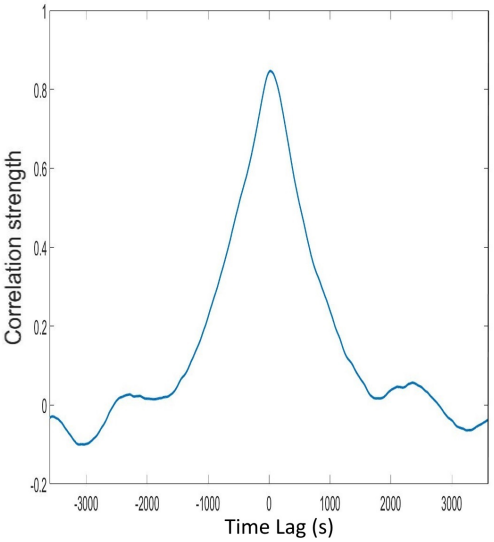

(c) This figure shows a lag vs. correlation plot for the thermistors 1 and 4 of the Bottom plate. Figure 5 shows the location of these two thermistors.. There is a strong dominant peak at $t \approx 0$ s and this peak is very smooth. This indicates a strong cross-correlation.

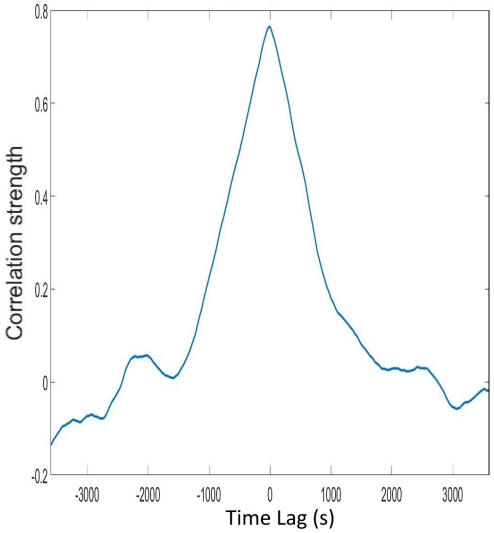

(d) This figure shows a lag vs. correlation plot for the thermistors 3 and 6 of the Bottom plate. Figure 5 shows the location of these two thermistors. There is a strong dominant peak at $t \approx 0$ s and this peak is very smooth. This indicates a strong cross-correlation.

Figure 12: Multiple graphs are shown which give the time lag vs. correlation strength of multiple thermistor pairs for the bottom and top plate. Graph a and b are graphs of the top plate and c and d are graphs of the bottom plate. These graphs are taken for case 10, however these graphs are somewhat representative for other rotating cases. For cases with higher Q for the bottom plate the main peak becomes sharper. The top plate becomes less periodic for high Q and for thermistor pairs 1vX and 5vX (X is any thermistor that is not 1 or 5) anticorrelation is observed

the vertical direction. The regimes mentioned in chapter 2 do not speak of a radial or azimuthal flow. the current data is not solid enough to confirm this, but it gives no indication that such flows are present in the TROCONVEX for any of its cases. More thermistors should be installed into the side walls so that possible azimuthal flow can be found or ruled out. Temperature measurements inside the centre fo the bulk could give better insight into possible radial flows.

Table 2: In this table the theoretical time scales for each case that is examined are found. The definitions of these time scales are found in chapter 2 and equation (2). t_{VAC}, t_{MAC}, t_{CIA} are time scales that are depended on rotation which means that for the non-rotating cases 1 through 7 these time scales hold no information. This is made clear by the X in the table.

Case	τ_{ff} (s)	t_{VAC} (s)	t_{MAC} (s)	t_{CIA} (s)
1	27.25	X	X	X
2	20.31	X	X	X
3	14.54	X	X	X
4	11.22	X	X	X
5	8.62	X	X	X
6	6.08	X	X	X
7	4.65	X	X	X
8	26.99	41.95	106.82	60.60
9	20.59	29.84	75.98	46.11
10	11.04	13.37	34.03	24.25
11	5.99	5.95	15.16	12.70
12	4.64	4.20	10.70	9.61
13	7.54	16.87	57.90	25.97

For same-side thermistors correlations are found for all cases. For the non-rotational low wattage cases the time scales are long and the direction is opposite between the top half of the thermistors and the bottom half. For these cases the time scales tend to be the same between each thermistor. The time scales are much longer than the theoretical time scales that are included in table 2. For the other non-rotational cases the time scales of the thermistors closer to the plate are shorter than for the thermistors closer to the centre. The top half and bottom half have an opposite direction of lag. The bottom half thermistors of Side A however do give results not compatible with that of the other thermistors. The time lag between A1 and A2 is much longer than the lag between A2 and A3. The direction of flow also changes between these two pairs. Neither of these results are observed for any other thermistor pair. Likely the effects caused by the room temperature peaks mentioned in chapter 4 have some impact on the measurements of thermistor A2. For the higher wattage cases the time scales' direction suggest a large scale circulation like figure 3a. However the length of these time scales would be too long for an LSC.

For all rotational cases a similar pattern of time scales is found. The thermistors closer to the plates give shorter time lags compared to the other thermistors. The time lags shorten for higher wattage cases as expected, but still the time scales are larger than the theoretical time scales. Case 13 is the only one where the theory and the results seem to agree. Figure 13 shows the time lags of Side B for Case 13 across the entire segmented measurement. This is done in order to observe if the time scales change direction or length. Because thermistor A2 giving wrong results this graph is not made for Side A. Both the direction and length of the time lags do not change significantly. Given these time lags a flow structure as shown in figure 14 is a possibility. This kind of flow structure would explain why Side A has shorter time scales compared to Side B, at least for the thermistors close to the top plate. This flow structure also explains the directional differences between the top and bottom half of the tank. For the other rotational cases this kind of flow structure is also possible. However this flow structure cannot explain why the time lags are significantly shorter than theorized.

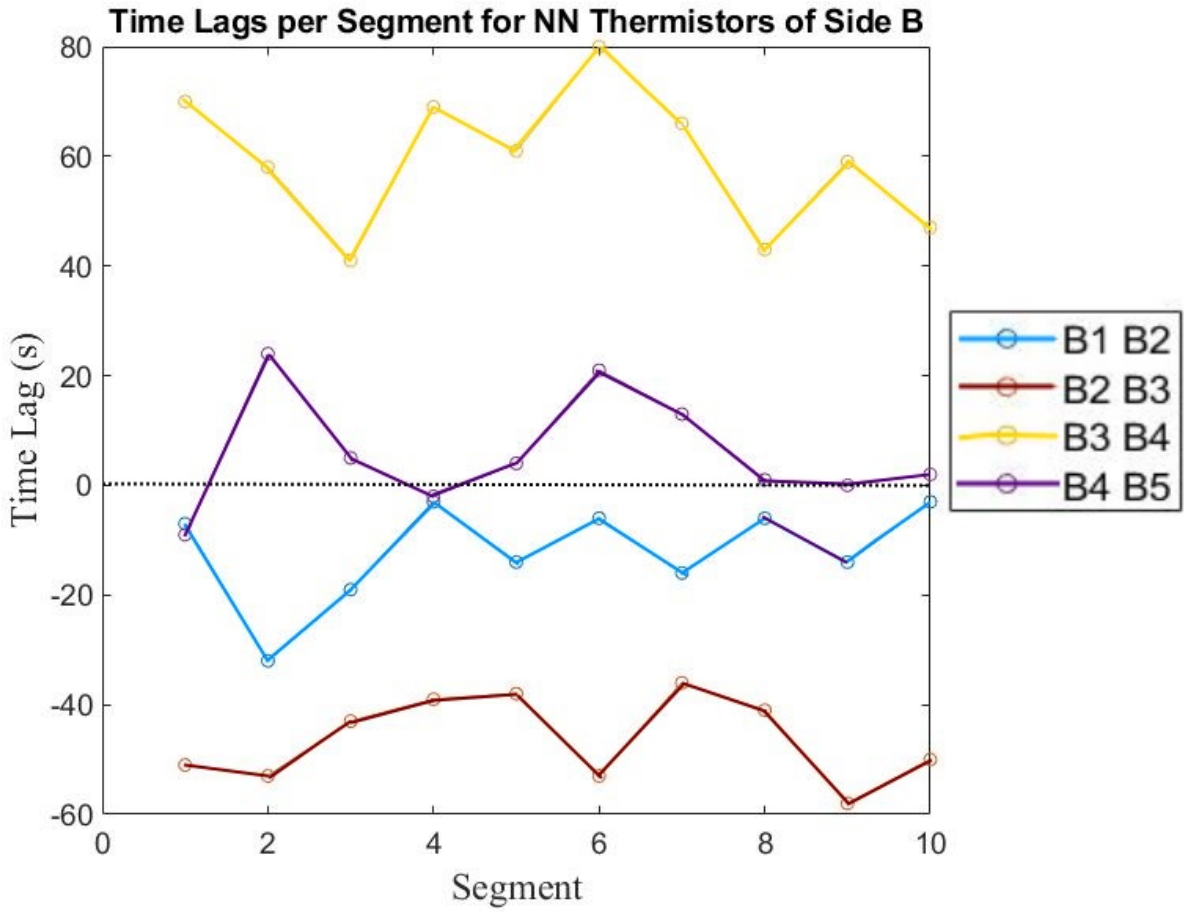

Figure 13: This figure shows for each segmented the corresponding time lags are plotted of Side B for Case 13. The thermistors located closer to the plates have shorter time lags than the other thermistors. For thermistor with $z < H/2$ the time lags are negative while for the thermistors $z > H/2$ the time lags are positive.

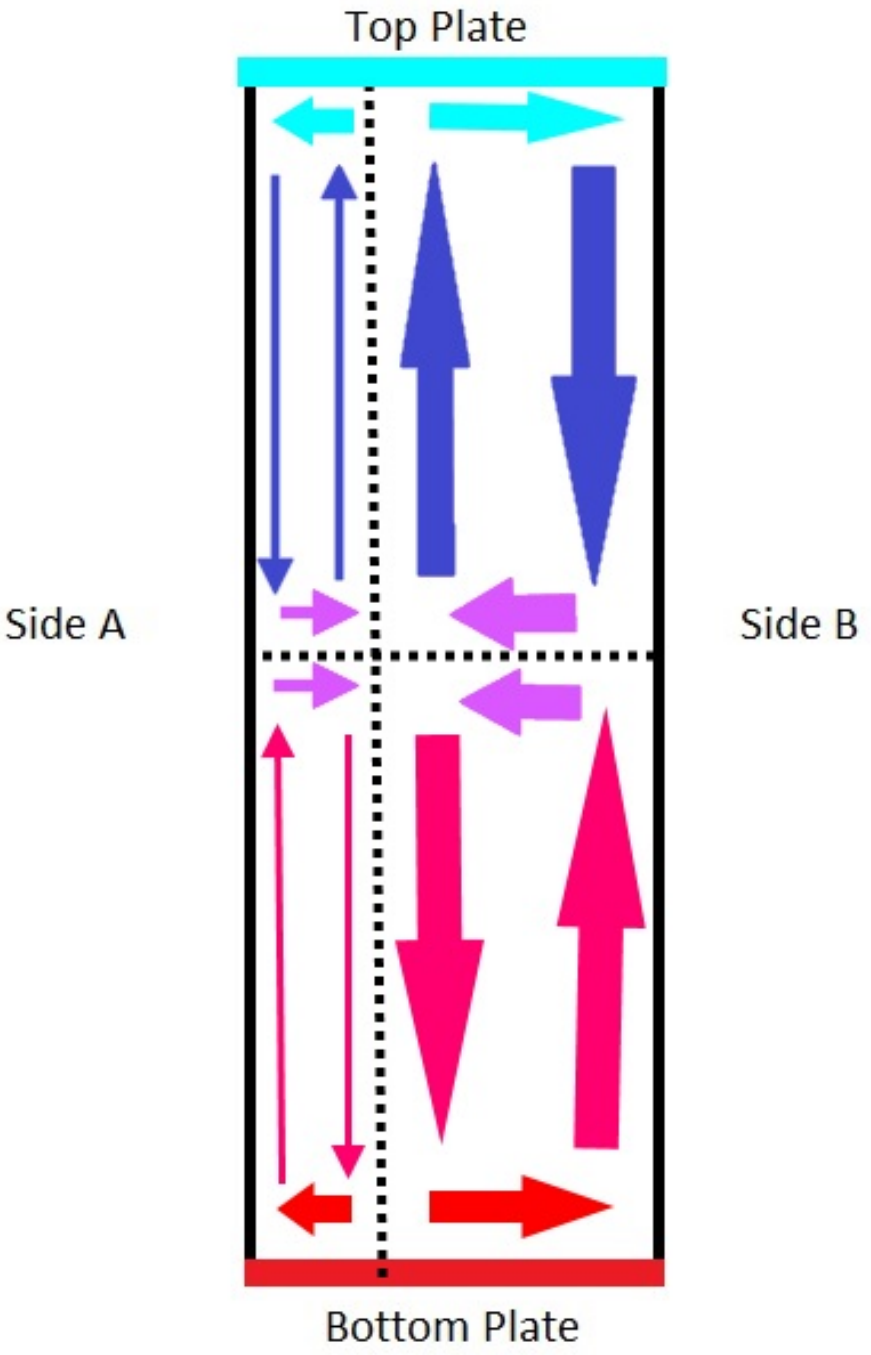

Figure 14: This sketch shows a possible flow structure for the rotational cases especially for Case 13. The thermistors located closer to the plates have shorter time lags than the other thermistors. Side A has shorter time lags compared to Side B and this could be explained by having the rolls which are next to each other to be of different size. For $z < H/2$ the flow direction is upwards while for $z > H/2$ the direction is downwards. The colour of the arrows give an indication of the local temperature.

6 Conclusion

In order to gain a better understanding of Rayleigh Bérnard Convection Fourier spectrum analysis as well as cross-correlations are used on thermal data taken from the TROCONVEX. The Fourier spectrum analysis shows that a frequency $f_{room} \approx \Omega$ appears at the top plate for all cases. This frequency is also present for three side wall thermistors namely A2, A3 and B3. This is not flow related and instead means that the top plate and these three thermistors are not well isolated and that envrironmental effects affect the data. The method of cooling for the top plate for the lower wattage cases can also be identified via Fourier. The chiller that cools the top plate does this with a frequency $f_{chiller} = 1.11$ mHz and a bump is located at $f_{chiller}$ in the power spectrum for the top plate thermal data. Fourier analysis on the bottom plate and the other side wall thermistors do not show any interesting or peculiar peaks in the Fourier space.

The influence of the chiller on the top plate can be reduced by using a filter to remove the unwanted frequency $f_{chiller}$. The environmental cause of f_{room} should, if possible, be identified and dealt with. Alternatively the TROCONVEX could be shielded from this unwanted cooling or a multiband filter can be used to remove the unwanted frequencies. The isolation for the side wall thermistors A2, A3 and B3 should be improved as well as checking if these thermistors are sufficiently in contact with the fluid. The bottom plate and the remaining thermistor seem to have no issues regarding isolation therefore no improvements have to made for these devices. No conclusions based on the Fourier spectrum analysis for flow structures can be made.

Cross-correlations show for the bottom plate short time lags are found. The direction in which the fluid should flow according to these time lags is inconsistent and suggests that these time lags are not flow related. There is no appreciable difference between any of the cases and no thermistor pair stands out. It is highly unlikely that outside influences are the main cause for these time lags. However the results could indicate that the layer of fluid on top of the plate is of uniform temperature. The thermal variations happen at the same time across the whole plate. It can also not be excluded that boundary layer are the cause of these results, but more insight in the nature of this boundary layer is needed first. The time lags for the top plate are in general shorter than those for the bottom plate. Here the direction of flow changes inconsistently. The periodicity found in the *time lag vs. correlation strength* plots hints strongly toward the unwanted frequencies f_{room} and $f_{chiller}$ influencing the data and therefore the found time lags. However removing these frequencies will not necessarily result in more reasonable time lags. This is because similar issues that occur at the bottom plate can be present at the top plate as well.

From the results of the cross-correlation on thermal from the side walls a flow structure similar to that of figure 3a could be deduced for the non-rotational cases. For the rotational cases a flow structure similar to that of figure 14 could be deduced. It is also observed that thermistor A2 is not measuring temperature properly. The time lags associated with this thermistor are not comparable with the other thermistors. Fourier analysis has already showed that this thermistor is affected by environmental influences and the correlation results confirm that this thermistor's isolation should be improved. That also means that the flow structure at the bottom corner at side A is unclear. Figures 3a and 14 are based on the assumption that this corner should have a flow structure that is similar as for the other corners so that symmetry is preserved. The time scales that are found are usually larger than the theoretical values. Not enough data is available to give a reason as to why this is the case. Maybe the flow structure has an azimuthal component to it which causes the flow to appear slower than expected. By adding more thermistors into the side wall this type of flow could be identified. From the results it is theorized that the rolls on one side of the tank are compressed in the horizontal direction while the rolls on the other side are expanded in this direction. Thermal measurements of the centre of the bulk could confirm or deny this flow structure.

A Time tables of the Top & Bottom plate

A.1 Explanation of the tables

The tables hold information about the time lags and correlation strength of all thermistor pairs of the top and bottom plate. The combination of the column and row number gives the examined thermistor pair. Let r be the row number and c be the column number then cell (r,c) gives the correlation between thermistors r and c. For the cells where $r = c$ the autocorrelation is given. The numbers r and c directly correspond with the thermistor numbering as is explained in chapter 3 and figure 5. For example row 2, column 5 gives the correlation between thermistor 2 and 5. The correlation strength ranges from -1 to 1. The further away from 0, the stronger the (anti-)correlation for that particular thermistor pair. A red box indicates a correlation that is considered weak or non-existing and the found time lags removed from the tables. The 1's left of the diagonal are the mirror image of the actual time lags and these are not given.

A.2 Time tables for the non-rotating cases

Timelags of Top

	1	2	3	4	5	6	7
1							
2	1						
3	1	1					
4	1	1	1	0			
5	1	1	1	1			
6	1	1	1	1	1		
7	1	1	1	1	1	1	

Peakstrengh of Top

	1	2	3	4	5	6	7
1	0.1167	0.0948	0.0830	0.1006	0.0966	0.0807	0.0911
2	1	0.1009	0.0845	0.0861	0.0889	0.0864	0.0914
3	1	1	0.1001	0.0980	0.0739	0.0802	0.0800
4	1	1	1	0.1411	0.0627	0.0646	0.0740
5	1	1	1	1	0.1106	0.0987	0.0999
6	1	1	1	1	1	0.1168	0.0998
7	1	1	1	1	1	1	0.1081

Timelags of Bottom

	1	2	3	4	5	6	7	8
1	0	11	27	56	34	36	-4	0
2	1	0	28	25	30	37	-6	0
3	1	1	0	14	-18	-20	-69	-51
4	1	1	1	0	-72	-17	-111	-47
5	1	1	1	1	0	0	-24	-38
6	1	1	1	1	1	0	-39	-17
7	1	1	1	1	1	1	0	8
8	1	1	1	1	1	1	1	0

Peakstrengh of Bottom

	1	2	3	4	5	6	7	8
1	0.6722	0.5952	0.6563	0.5878	0.6012	0.5475	0.6155	0.5701
2	1	0.6677	0.5618	0.6471	0.5407	0.5872	0.5727	0.6009
3	1	1	0.6906	0.5608	0.5948	0.5024	0.5924	0.5286
4	1	1	1	0.6754	0.5230	0.5732	0.5492	0.5815
5	1	1	1	1	0.6895	0.5692	0.6569	0.5786
6	1	1	1	1	1	0.6752	0.5869	0.6540
7	1	1	1	1	1	1	0.6792	0.6039
8	1	1	1	1	1	1	1	0.6737

Figure A.2.1: The time lags are given for case 1 in these tables in seconds as well as the strength of the correlations for each thermistor pair r and c. For this case the autocorrelations that are found are weak.

Timelags of Top

	1	2	3	4	5	6	7
1	0	-5	-6	-13	-6	-8	-9
2	1	0	-1	-4	0	-3	-3
3	1	1	0	-3	0	-3	-4
4	1	1	1	0	7	5	0
5	1	1	1	1	0	-2	-3
6	1	1	1	1	1	0	-2
7	1	1	1	1	1	1	0

Peakstrengh of Top

	1	2	3	4	5	6	7
1	0.5703	0.4618	0.4303	0.4251	0.5523	0.4410	0.4657
2	1	0.5814	0.4590	0.4133	0.4732	0.4501	0.4649
3	1	1	0.5973	0.4539	0.4459	0.4581	0.4610
4	1	1	1	0.5743	0.4368	0.4287	0.4789
5	1	1	1	1	0.5644	0.4618	0.4835
6	1	1	1	1	1	0.5954	0.4865
7	1	1	1	1	1	1	0.5722

Timelags of Bottom

	1	2	3	4	5	6	7	8
1	0	26	25	42	90		38	-3
2	1	0	-9	31		56	11	27
3	1	1	0	4	66		25	-37
4	1	1	1	0		12		-33
5	1	1	1	1	0	-68	-19	-111
6	1	1	1	1	1	0	112	-15
7	1	1	1	1	1	1	0	-94
8	1	1	1	1	1	1	1	0

Peakstrengh of Bottom

	1	2	3	4	5	6	7	8
1	0.7029	0.3954	0.6513	0.3760	0.2410	0.0417	0.2599	0.1907
2	1	0.6342	0.3355	0.5396	0.0382	0.2752	0.1647	0.3364
3	1	1	0.7712	0.2991	0.2130	0.0332	0.2313	0.1206
4	1	1	1	0.6512	0.0200	0.2216	0.0878	0.2848
5	1	1	1	1	0.7133	0.1511	0.5772	0.2404
6	1	1	1	1	1	0.7131	0.1598	0.5948
7	1	1	1	1	1	1	0.7242	0.2468
8	1	1	1	1	1	1	1	0.6771

Figure A.2.2: The time lags are given for case 2 in these tables in seconds as well as the strength of the correlations for each thermistor pair r and c. The correlations for the top plate are stronger for this case compared to the other 0RPM cases.

Timelags of Top

	1	2	3	4	5	6	7
1	0				0		
2	1	0					
3	1	1	0				
4	1	1	1	0			
5	1	1	1	1	0		
6	1	1	1	1	1	0	
7	1	1	1	1	1	1	0

Peakstrengh of Top

	1	2	3	4	5	6	7
1	0.1460	0.0954	0.0967	0.0749	0.1373	0.0772	0.0762
2	1	0.1428	0.1107	0.0977	0.0989	0.0985	0.0976
3	1	1	0.1862	0.0943	0.1069	0.0991	0.0787
4	1	1	1	0.1774	0.0777	0.1150	0.1135
5	1	1	1	1	0.2341	0.0437	0.0991
6	1	1	1	1	1	0.2737	0.1139
7	1	1	1	1	1	1	0.1988

Timelags of Bottom

	1	2	3	4	5	6	7	8
1	0	-10	25	39	24	22	-16	15
2	1	0	52	22	4	44	-5	16
3	1	1	0	-10	-11		-53	4
4	1	1	1	0	-596	-4	-36	-36
5	1	1	1	1	0	0	-18	-19
6	1	1	1	1	1	0	-32	-17
7	1	1	1	1	1	1	0	13
8	1	1	1	1	1	1	1	0

Peakstrengh of Bottom

	1	2	3	4	5	6	7	8
1	0.7464	0.5340	0.7091	0.4910	0.5023	0.3840	0.5377	0.4834
2	1	0.7583	0.4888	0.6833	0.3588	0.4345	0.4518	0.4924
3	1	1	0.7975	0.4565	0.4516	0.0193	0.4800	0.3914
4	1	1	1	0.7960	0.2646	0.4246	0.3627	0.4662
5	1	1	1	1	0.8283	0.4934	0.7273	0.5051
6	1	1	1	1	1	0.7920	0.4897	0.6834
7	1	1	1	1	1	1	0.7836	0.5400
8	1	1	1	1	1	1	1	0.7438

Figure A.2.3: The time lags are given for case 3 in these tables in seconds as well as the strength of the correlations for each thermistor pair r and c.

Timelags of Top

	1	2	3	4	5	6	7
1	0	0	-2		5		
2	1	0	-2	-7		-3	
3	1	1	0	-4	8	4	
4	1	1	1	0		0	8
5	1	1	1	1	0		-2
6	1	1	1	1	1	0	2
7	1	1	1	1	1	1	0

Peakstrengh of Top

	1	2	3	4	5	6	7
1	0.2957	0.1768	0.1517	0.0940	0.2047	0.0949	0.0855
2	1	0.3623	0.1541	0.1731	0.1182	0.1569	0.1081
3	1	1	0.4242	0.1408	0.1256	0.2156	0.0812
4	1	1	1	0.4030	0.0609	0.1805	0.1497
5	1	1	1	1	0.4757	-0.0188	0.1814
6	1	1	1	1	1	0.5775	0.1254
7	1	1	1	1	1	1	0.3918

Timelags of Bottom

	1	2	3	4	5	6	7	8
1	0	-32	20	11			-57	
2	1	0	59	19			-24	20
3	1	1	0	-11				
4	1	1	1	0				
5	1	1	1	1	0		-16	
6	1	1	1	1	1	0		-14
7	1	1	1	1	1	1	0	
8	1	1	1	1	1	1	1	0

Peakstrengh of Bottom

	1	2	3	4	5	6	7	8
1	0.8218	0.3045	0.6053	0.2257	0.0861	0.0399	0.1807	0.1196
2	1	0.8184	0.2375	0.6044	0.0469	0.0827	0.1688	0.1386
3	1	1	0.7945	0.1852	0.0070	0.0496	0.0805	0.0522
4	1	1	1	0.7431	0.0230	0.1102	0.0222	0.1172
5	1	1	1	1	0.8401	0.0803	0.6802	0.0921
6	1	1	1	1	1	0.7468	0.0812	0.5870
7	1	1	1	1	1	1	0.8393	0.1065
8	1	1	1	1	1	1	1	0.7467

Figure A.2.4: The time lags are given for case 4 in these tables in seconds as well as the strength of the correlations for each thermistor pair r and c.

Timelags of Top

	1	2	3	4	5	6	7
1	0	-2			6		
2	1	0		-3			
3	1	1	0			13	
4	1	1	1	0		16	11
5	1	1	1	1	0		
6	1	1	1	1	1	0	
7	1	1	1	1	1	1	0

Peakstrengh of Top

	1	2	3	4	5	6	7
1	0.2365	0.1292	0.0587	0.0875	0.1213	0.0496	0.0411
2	1	0.3073	0.0982	0.1413	0.0564	0.0852	0.0621
3	1	1	0.5145	0.0904	0.0786	0.2202	0.0789
4	1	1	1	0.4530	0.0506	0.1357	0.1593
5	1	1	1	1	0.4154	-0.0455	0.1162
6	1	1	1	1	1	0.6480	0.1137
7	1	1	1	1	1	1	0.3441

Timelags of Bottom

	1	2	3	4	5	6	7	8
1	0	11	18	45	8	14	0	0
2	1	0	6	18	-283		0	
3	1	1	0	29	0		-15	0
4	1	1	1	0	-426	-15	-8	-40
5	1	1	1	1	0	387	-14	-231
6	1	1	1	1	1	0	-50	-13
7	1	1	1	1	1	1	0	16
8	1	1	1	1	1	1	1	0

Peakstrengh of Bottom

	1	2	3	4	5	6	7	8
1	0.7518	0.2678	0.6056	0.2450	0.3728	0.3625	0.4454	0.4332
2	1	0.6439	0.1862	0.4575	0.2324	0.0043	0.3493	0.0364
3	1	1	0.7953	0.1395	0.2221	0.0693	0.4116	0.2905
4	1	1	1	0.7481	0.1548	0.2389	0.2300	0.2341
5	1	1	1	1	0.7660	0.1922	0.5829	0.3123
6	1	1	1	1	1	0.7116	0.3337	0.5251
7	1	1	1	1	1	1	0.7219	0.3860
8	1	1	1	1	1	1	1	0.7741

Figure A.2.5: The time lags are given for case 5 in these tables in seconds as well as the strength of the correlations for each thermistor pair r and c.

Timelags of Top

	1	2	3	4	5	6	7
1	0	17	11	12	9	10	
2	1	0	-4	-5	-6	-5	-3
3	1	1	0	-3	-1	1	0
4	1	1	1	0	-2	0	3
5	1	1	1	1	0		1
6	1	1	1	1	1	0	2
7	1	1	1	1	1	1	0

Peakstrengh of Top

	1	2	3	4	5	6	7
1	0.6910	0.1265	0.2094	0.1313	0.3423	0.1703	-0.0101
2	1	0.5220	0.2955	0.3323	0.1489	0.2540	0.3486
3	1	1	0.5595	0.2786	0.2309	0.2625	0.2525
4	1	1	1	0.5631	0.1529	0.2642	0.3591
5	1	1	1	1	0.7070	0.0558	0.1854
6	1	1	1	1	1	0.6285	0.2754
7	1	1	1	1	1	1	0.5752

Timelags of Bottom

	1	2	3	4	5	6	7	8
1	0	-10	14	0	-13	-16	-33	
2	1	0	56	13		-18		2
3	1	1	0	-20	-14		-37	
4	1	1	1	0		12		8
5	1	1	1	1	0	-8	-12	
6	1	1	1	1	1	0	0	-8
7	1	1	1	1	1	1	0	
8	1	1	1	1	1	1	1	0

Peakstrengh of Bottom

	1	2	3	4	5	6	7	8
1	0.8094	0.2265	0.6464	0.1432	0.2454	0.1572	0.1766	0.0291
2	1	0.8133	0.1459	0.5219	0.1020	0.2061	0.0884	0.1652
3	1	1	0.8341	0.1372	0.2378	0.0551	0.1573	0.0966
4	1	1	1	0.7485	-0.0087	0.2161	-0.0073	0.1409
5	1	1	1	1	0.8326	0.2183	0.6332	0.0945
6	1	1	1	1	1	0.8071	0.1356	0.5068
7	1	1	1	1	1	1	0.8080	0.0398
8	1	1	1	1	1	1	1	0.6682

Figure A.2.6: The time lags are given for case 6 in these tables in seconds as well as the strength of the correlations for each thermistor pair r and c. The correlations for the top plate are stronger for this case compared to the other 0RPM cases.

Timelags of Top

	1	2	3	4	5	6	7
1	0				10		
2	1	0	0	-8		-8	0
3	1	1	0	-7	1	1	0
4	1	1	1	0		-1	6
5	1	1	1	1	0		
6	1	1	1	1	1	0	4
7	1	1	1	1	1	1	0

Peakstrengh of Top

	1	2	3	4	5	6	7
1	0.7407	0.0120	0.0909	0.0195	0.2552	0.0225	-0.0558
2	1	0.4177	0.1400	0.1693	0.0292	0.1202	0.2049
3	1	1	0.5883	0.1359	0.1809	0.2016	0.1555
4	1	1	1	0.5347	0.0122	0.1711	0.2663
5	1	1	1	1	0.6591	-0.0461	0.0993
6	1	1	1	1	1	0.6127	0.1985
7	1	1	1	1	1	1	0.5303

Timelags of Bottom

	1	2	3	4	5	6	7	8
1	0	-10	12	-22	-1	-12	-12	5
2	1	0	78	11	3	-10	5	-29
3	1	1	0	-21	13		-32	5
4	1	1	1	0		-7		0
5	1	1	1	1	0	-21	-9	-20
6	1	1	1	1	1	0	34	-7
7	1	1	1	1	1	1	0	-3
8	1	1	1	1	1	1	1	0

Peakstrengh of Bottom

	1	2	3	4	5	6	7	8
1	0.8333	0.2068	0.6265	0.1720	0.2902	0.1800	0.2609	0.1843
2	1	0.7955	0.1695	0.5638	0.1315	0.2785	0.1758	0.2678
3	1	1	0.8597	0.1642	0.2832	0.0781	0.2311	0.1683
4	1	1	1	0.8515	0.0387	0.3545	0.1105	0.2952
5	1	1	1	1	0.8854	0.1928	0.6510	0.1666
6	1	1	1	1	1	0.8422	0.1687	0.6053
7	1	1	1	1	1	1	0.8663	0.1838
8	1	1	1	1	1	1	1	0.8426

Figure A.2.7: The time lags are given for case 7 in these tables in seconds as well as the strength of the correlations for each thermistor pair r and c.

A.3 Time tables for the rotating cases

Timelags of Top

	1	2	3	4	5	6	7
1	0	-1	-1	-4	-3	-4	-8
2	1	0	-1	-3	-1	-3	-3
3	1	1	0	-2	-1	-3	-3
4	1	1	1	0	2	0	1
5	1	1	1	1	0	-2	-2
6	1	1	1	1	1	0	0
7	1	1	1	1	1	1	0

Peakstrengh of Top

	1	2	3	4	5	6	7
1	0.4499	0.3911	0.3576	0.3706	0.4085	0.4105	0.4101
2	1	0.4395	0.3764	0.3550	0.3847	0.4120	0.4079
3	1	1	0.4467	0.3673	0.3439	0.3943	0.3940
4	1	1	1	0.4326	0.3512	0.3693	0.3817
5	1	1	1	1	0.5551	0.4010	0.4000
6	1	1	1	1	1	0.4517	0.4245
7	1	1	1	1	1	1	0.4545

Timelags of Bottom

	1	2	3	4	5	6	7	8
1	0	25	10	24	-7	20	-24	0
2	1	0	-6	10	19	39	9	43
3	1	1	0	8	0	6	0	-1
4	1	1	1	0	0	27	0	34
5	1	1	1	1	0	-10	-7	-16
6	1	1	1	1	1	0	23	-8
7	1	1	1	1	1	1	0	-34
8	1	1	1	1	1	1	1	0

Peakstrengh of Bottom

	1	2	3	4	5	6	7	8
1	0.7562	0.6900	0.7426	0.6935	0.6866	0.6600	0.6844	0.6450
2	1	0.7598	0.6956	0.7395	0.6806	0.6916	0.6708	0.6848
3	1	1	0.7622	0.6996	0.6936	0.6763	0.6895	0.6618
4	1	1	1	0.7653	0.6973	0.7025	0.6867	0.6946
5	1	1	1	1	0.7540	0.7024	0.7349	0.7005
6	1	1	1	1	1	0.7497	0.6932	0.7298
7	1	1	1	1	1	1	0.7501	0.6952
8	1	1	1	1	1	1	1	0.7501

Figure A.3.1: The time lags are given for case 8 in these tables in seconds as well as the strength of the correlations for each thermistor pair r and c.

Timelags of Top

	1	2	3	4	5	6	7
1	0	-3	-2	-3	-3	-6	-12
2	1	0	-1	-3	-1	-4	-3
3	1	1	0	-2	-1	-3	-3
4	1	1	1	0	2	-1	2
5	1	1	1	1	0	-2	-3
6	1	1	1	1	1	0	1
7	1	1	1	1	1	1	0

Peakstrengh of Top

	1	2	3	4	5	6	7
1	0.5829	0.4448	0.3096	0.3689	0.5227	0.4234	0.3707
2	1	0.5965	0.3884	0.3795	0.4851	0.4746	0.3986
3	1	1	0.5737	0.3873	0.3635	0.4358	0.3947
4	1	1	1	0.6139	0.4286	0.4228	0.4799
5	1	1	1	1	0.5646	0.4868	0.4820
6	1	1	1	1	1	0.5753	0.4525
7	1	1	1	1	1	1	0.6313

Timelags of Bottom

	1	2	3	4	5	6	7	8
1	0	44	13	24	0	10	3	9
2	1	0	-22	10	-3	11	-21	4
3	1	1	0	10	0	-14	0	-14
4	1	1	1	0	-6	2	-25	-12
5	1	1	1	1	0	-16	-2	-16
6	1	1	1	1	1	0	27	0
7	1	1	1	1	1	1	0	-24
8	1	1	1	1	1	1	1	0

Peakstrengh of Bottom

	1	2	3	4	5	6	7	8
1	0.6319	0.5380	0.6019	0.5229	0.5428	0.4753	0.5526	0.4681
2	1	0.6188	0.5240	0.5745	0.5205	0.5261	0.5049	0.5121
3	1	1	0.6295	0.5078	0.5402	0.4759	0.5469	0.4658
4	1	1	1	0.5944	0.5239	0.5192	0.5111	0.5088
5	1	1	1	1	0.6148	0.5075	0.5937	0.5011
6	1	1	1	1	1	0.5863	0.4981	0.5568
7	1	1	1	1	1	1	0.6233	0.4945
8	1	1	1	1	1	1	1	0.5717

Figure A.3.2: The time lags are given for case 9 in these tables in seconds as well as the strength of the correlations for each thermistor pair r and c.

Timelags of Top

	1	2	3	4	5	6	7
1	0				1		-297
2	1	0	-9			-11	254
3	1	1	0	-29		-3	
4	1	1	1	0			4
5	1	1	1	1	0	-121	
6	1	1	1	1	1	0	
7	1	1	1	1	1	1	0

Peakstrengh of Top

	1	2	3	4	5	6	7
1	0.7810	-0.0349	-0.0328	0.0958	0.4683	-0.0180	-0.1229
2	1	0.6139	0.2084	0.0953	0.0378	0.1350	-0.1947
3	1	1	0.6534	0.1355	-0.0639	0.2684	-0.0445
4	1	1	1	0.6550	0.0897	0.0248	0.2534
5	1	1	1	1	0.8364	-0.1914	0.0344
6	1	1	1	1	1	0.7273	0.0125
7	1	1	1	1	1	1	0.7446

Timelags of Bottom

	1	2	3	4	5	6	7	8
1	0	12	11	23	0	4	3	2
2	1	0	-5	11	38	27	39	21
3	1	1	0	29	-35	-8	-16	-8
4	1	1	1	0	13	34	4	16
5	1	1	1	1	0	-59	-7	-64
6	1	1	1	1	1	0	45	0
7	1	1	1	1	1	1	0	-50
8	1	1	1	1	1	1	1	0

Peakstrengh of Bottom

	1	2	3	4	5	6	7	8
1	0.7623	0.6581	0.6828	0.6286	0.6076	0.5806	0.6323	0.6015
2	1	0.7821	0.6268	0.7326	0.5678	0.6522	0.6004	0.6704
3	1	1	0.7527	0.6236	0.5578	0.5120	0.5752	0.5456
4	1	1	1	0.8083	0.5556	0.6415	0.5944	0.6485
5	1	1	1	1	0.7800	0.6256	0.7263	0.6296
6	1	1	1	1	1	0.7991	0.6582	0.7482
7	1	1	1	1	1	1	0.7954	0.6718
8	1	1	1	1	1	1	1	0.7915

Figure A.3.3: The time lags are given for case 10 in these tables in seconds as well as the strength of the correlations for each thermistor pair r and c. The correlations for the top plate are weaker for this case compared to the other 3RPM cases.

Timelags of Top

	1	2	3	4	5	6	7
1	0	-133	-119	-141	4		
2	1	0	-4	-6	81	-9	
3	1	1	0	-6	87	-4	-11
4	1	1	1	0	94	1	0
5	1	1	1	1	0	-64	
6	1	1	1	1	1	0	-24
7	1	1	1	1	1	1	0

Peakstrengh of Top

	1	2	3	4	5	6	7
1	0.8261	-0.1936	-0.1226	-0.1398	0.3945	-0.1013	-0.0805
2	1	0.8763	0.5742	0.4921	-0.2664	0.3400	0.1119
3	1	1	0.8659	0.4465	-0.2347	0.4485	0.1767
4	1	1	1	0.8565	-0.2718	0.2805	0.4440
5	1	1	1	1	0.7907	-0.3541	-0.0872
6	1	1	1	1	1	0.8194	0.2136
7	1	1	1	1	1	1	0.8634

Timelags of Bottom

	1	2	3	4	5	6	7	8
1	0	11	2	12	0	16	-4	9
2	1	0	-5	5	3	6	-5	13
3	1	1	0	16	-5	8	-1	0
4	1	1	1	0	-2	9	-10	2
5	1	1	1	1	0	-6	-1	-2
6	1	1	1	1	1	0	0	1
7	1	1	1	1	1	1	0	0
8	1	1	1	1	1	1	1	0

Peakstrengh of Bottom

	1	2	3	4	5	6	7	8
1	0.8047	0.5506	0.6202	0.5062	0.4715	0.4746	0.4901	0.4887
2	1	0.8079	0.4940	0.6070	0.4123	0.4520	0.4579	0.5203
3	1	1	0.7994	0.5263	0.5102	0.4069	0.5105	0.4572
4	1	1	1	0.8417	0.3560	0.4753	0.4444	0.4283
5	1	1	1	1	0.8066	0.4522	0.6483	0.4796
6	1	1	1	1	1	0.7839	0.4806	0.6181
7	1	1	1	1	1	1	0.8148	0.5600
8	1	1	1	1	1	1	1	0.8317

Figure A.3.4: The time lags are given for case 11 in these tables in seconds as well as the strength of the correlations for each thermistor pair r and c.

Timelags of Top

	1	2	3	4	5	6	7
1	0		-117	-144	21	-98	-11
2	1	0	-4	-4	94	-26	
3	1	1	0	-8	137	-4	
4	1	1	1	0	146	20	2
5	1	1	1	1	0	-101	-126
6	1	1	1	1	1	0	-29
7	1	1	1	1	1	1	0

Peakstrengh of Top

	1	2	3	4	5	6	7
1	0.8057	-0.0473	-0.1297	-0.1577	0.3239	-0.1840	-0.1936
2	1	0.8774	0.4657	0.3900	-0.2897	0.3719	0.0373
3	1	1	0.7697	0.3944	-0.2372	0.4430	0.0992
4	1	1	1	0.7327	-0.2180	0.2811	0.2761
5	1	1	1	1	0.8570	-0.3676	-0.1744
6	1	1	1	1	1	0.8548	0.2372
7	1	1	1	1	1	1	0.8054

Timelags of Bottom

	1	2	3	4	5	6	7	8
1	0	9	-4	3	-6	-1	-7	12
2	1	0	-6	-4	8	-5	-4	8
3	1	1	0	3	-2	3	6	12
4	1	1	1	0	-4	0	-2	6
5	1	1	1	1	0	-1	4	9
6	1	1	1	1	1	0	11	7
7	1	1	1	1	1	1	0	-5
8	1	1	1	1	1	1	1	0

Peakstrengh of Bottom

	1	2	3	4	5	6	7	8
1	0.7226	0.4717	0.5971	0.4709	0.5261	0.4625	0.5277	0.3874
2	1	0.7616	0.4915	0.6127	0.4407	0.4617	0.3923	0.4624
3	1	1	0.7606	0.5157	0.5312	0.4381	0.5302	0.3843
4	1	1	1	0.8350	0.4726	0.5605	0.4784	0.4822
5	1	1	1	1	0.8168	0.5302	0.6838	0.4589
6	1	1	1	1	1	0.7741	0.5288	0.5978
7	1	1	1	1	1	1	0.8172	0.4979
8	1	1	1	1	1	1	1	0.7074

Figure A.3.5: The time lags are given for case 12 in these tables in seconds as well as the strength of the correlations for each thermistor pair r and c.

Timelags of Top

	1	2	3	4	5	6	7
1	0	-59			-2	-14	-10
2	1	0	-71				
3	1	1	0	-37	23	-7	23
4	1	1	1	0		-16	-4
5	1	1	1	1	0		68
6	1	1	1	1	1	0	
7	1	1	1	1	1	1	0

Peakstrengh of Top

	1	2	3	4	5	6	7
1	0.5759	0.1608	0.0252	0.0500	0.1739	0.1636	0.1445
2	1	0.5375	0.1431	0.0011	0.1156	0.0804	0.1025
3	1	1	0.6345	0.2218	0.1340	0.1615	0.1257
4	1	1	1	0.7651	0.0654	0.1210	0.2458
5	1	1	1	1	0.7593	-0.0207	0.2641
6	1	1	1	1	1	0.7569	0.1079
7	1	1	1	1	1	1	0.7132

Timelags of Bottom

	1	2	3	4	5	6	7	8
1	0	105	12	98	-49	-32	-85	236
2	1	0	-70	3	-133	79	-207	96
3	1	1	0	64	-58	23	-81	96
4	1	1	1	0	-40	52	-148	64
5	1	1	1	1	0	-52	-9	-86
6	1	1	1	1	1	0	55	-4
7	1	1	1	1	1	1	0	-86
8	1	1	1	1	1	1	1	0

Peakstrengh of Bottom

	1	2	3	4	5	6	7	8
1	0.8000	0.5736	0.7332	0.5246	0.5983	0.3701	0.5467	0.3167
2	1	0.7886	0.5858	0.7042	0.4342	0.5133	0.3792	0.5273
3	1	1	0.7926	0.5817	0.5766	0.4650	0.5177	0.3846
4	1	1	1	0.7622	0.4404	0.5565	0.3766	0.5407
5	1	1	1	1	0.7935	0.5484	0.7209	0.4762
6	1	1	1	1	1	0.7869	0.5564	0.7118
7	1	1	1	1	1	1	0.7843	0.5317
8	1	1	1	1	1	1	1	0.7772

Figure A.3.6: The time lags are given for case 13 in these tables in seconds as well as the strength of the correlations for each thermistor pair r and c.

B Time tables of the Side walls

B.1 Explanation of the tables

The tables hold information about the time lags and correlation strength of all thermistor pairs of Side A and Side B. The combination of the column and row number gives the examined thermistor pair. Let r be the row number and c be the column number then cell (r,c) gives the correlation between thermistors r and c. For the cells where $r = c$ the autocorrelation is given. The numbers r and c directly correspond with the thermistor numbering as is explained in chapter 3 and figure 4. For example row 2, column 3 gives the correlation between thermistor 2 and 3. Only the correlations between nearest neighbours thermistor pairs are examined, because other thermistor pairs gave weak correlations or time lags that are too long for RBC. The correlation strength ranges from -1 to 1. The further away from 0, the stronger the (anti-)correlation for that particular thermistor pair. A red box indicates a correlation that is considered weak or non-existing and the found time lags removed from the tables. The 1's left of the diagonal are the mirror image of the actual time lags and these are not given.

The tables called *Time-Peakstrength of the Sides* are somewhat different. Here the column number c refers to the thermistor number for both side A and B. This means that column c gives the time lags and strengths for the correlation between thermistor c of side A as well as thermistor c of side B. For example column 2 of these tables gives the correlation between thermistor A2 and B2. Chapter 3 and figure 4 give the exact location of these thermistors. For these tables row 1 gives the time lags while row 2 gives the correlation strength.

B.2 Time tables for the non-rotating cases

Timelags of SideB

	1	2	3	4	5
1	0	-217			
2	1	0	-164		
3	1	1	0	167	
4	1	1	1	0	0
5	1	1	1	1	0

Peakstrengh of SideB

	1	2	3	4	5
1	0.8309	0.1233	0.0228	0.1300	0.0139
2	1	0.7915	0.3771	0.3014	0.2133
3	1	1	0.4456	0.3869	0.3017
4	1	1	1	0.7077	0.3532
5	1	1	1	1	0.7333

Time-Peakstrengh of the Sides

	1	2	3	4	5
1				-3223	499
2	0.0014	0.0501	0.1104	0.2473	0.2277

Timelags of SideA

	1	2	3	4	5
1	0	-249			
2	1	0	0		
3	1	1	0	274	
4	1	1	1	0	198
5	1	1	1	1	0

Peakstrengh of SideA

	1	2	3	4	5
1	0.7864	0.1375	0.3051	0.1657	0.2521
2	1	0.7143	0.2803	0.2862	0.2179
3	1	1	0.7226	0.2691	0.0384
4	1	1	1	0.7599	0.3382
5	1	1	1	1	0.7667

Figure B.2.1: The time lags are given for case 1 in these tables as well as the strength of the correlations for each thermistor pair.

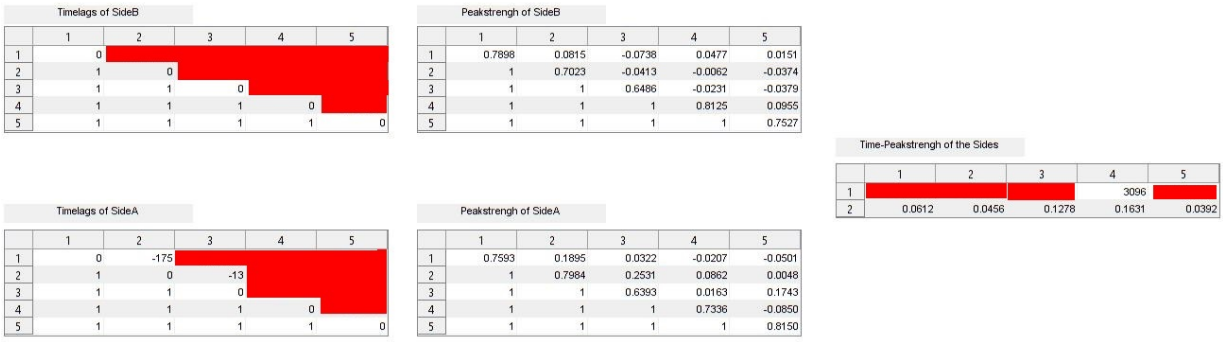

Figure B.2.2: The time lags are given for case 2 in these tables as well as the strength of the correlations for each thermistor pair.

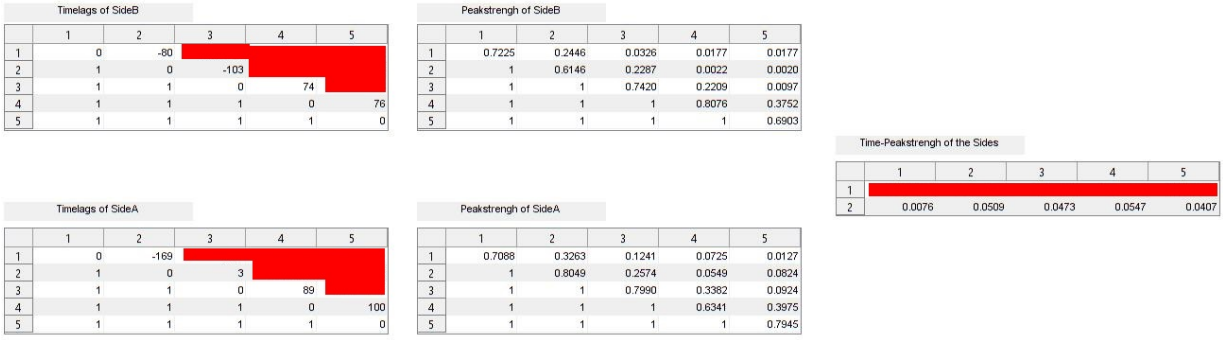

Figure B.2.3: The time lags are given for case 3 in these tables as well as the strength of the correlations for each thermistor pair.

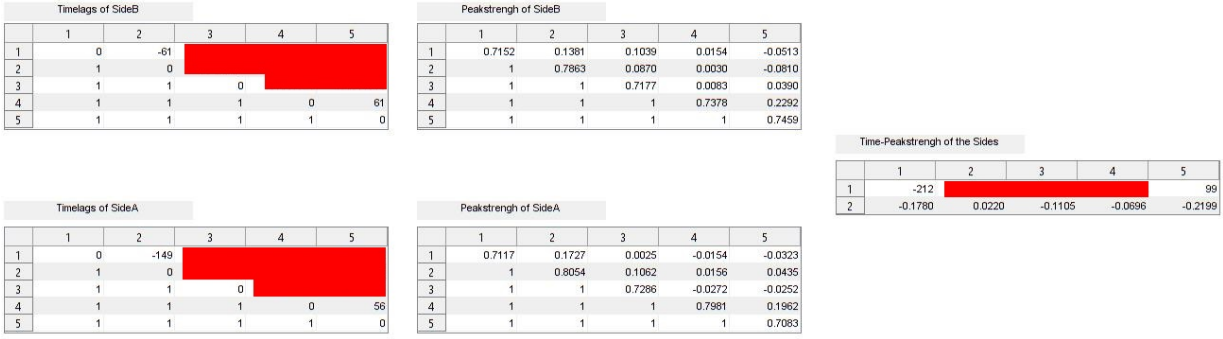

Figure B.2.4: The time lags are given for case 4 in these tables as well as the strength of the correlations for each thermistor pair.

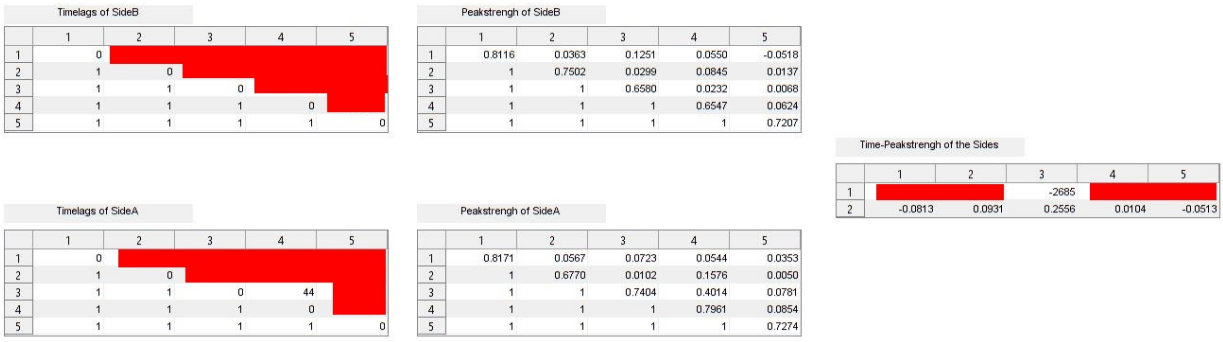

Figure B.2.5: The time lags are given for case 5 in these tables as well as the strength of the correlations for each thermistor pair.

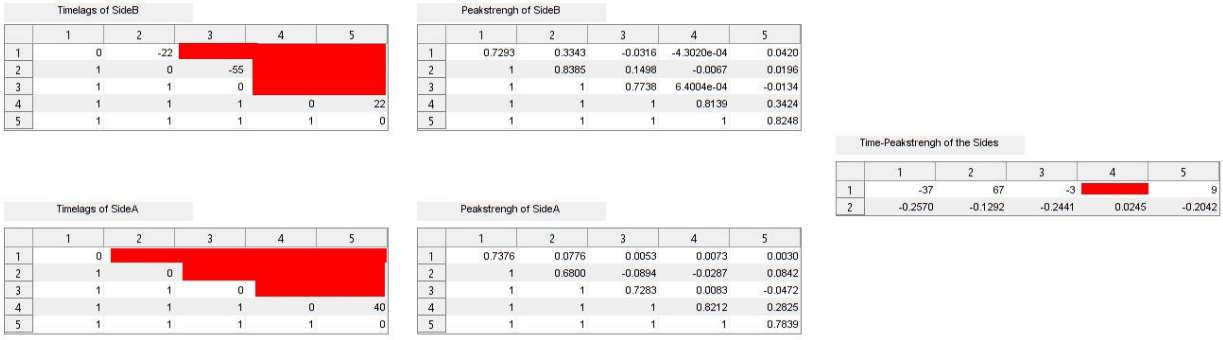

Figure B.2.6: The time lags are given for case 6 in these tables as well as the strength of the correlations for each thermistor pair.

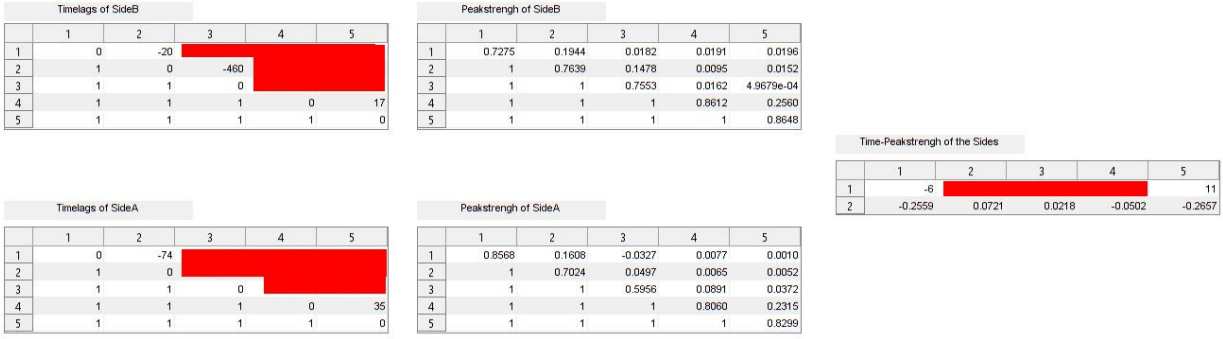

Figure B.2.7: The time lags are given for case 7 in these tables as well as the strength of the correlations for each thermistor pair.

B.3 Time tables for the rotating cases

Timelags of SideB

	1	2	3	4	5
1	0	-38			
2	1	0	-82		
3	1	1	0	87	
4	1	1	1	0	39
5	1	1	1	1	0

Peakstrengh of SideB

	1	2	3	4	5
1	0.6799	0.4473	0.3469	0.2375	0.0102
2	1	0.6811	0.3879	0.2851	0.0965
3	1	1	0.6354	0.4183	0.0423
4	1	1	1	0.7264	0.3367
5	1	1	1	1	0.8117

Time-Peakstrengh of the Sides

	1	2	3	4	5
1		95	-37	5	
2	0.1121	-0.1498	-0.3576	-0.2016	-0.0126

Timelags of SideA

	1	2	3	4	5
1	0	-100			
2	1	0	20		
3	1	1	0	57	
4	1	1	1	0	10
5	1	1	1	1	0

Peakstrengh of SideA

	1	2	3	4	5
1	0.7652	0.3385	0.2440	0.0358	-0.0053
2	1	0.7346	0.5663	0.2995	0.1737
3	1	1	0.7614	0.5281	0.3479
4	1	1	1	0.7867	0.5386
5	1	1	1	1	0.7839

Figure B.3.1: The time lags are given for case 8 in these tables as well as the strength of the correlations for each thermistor pair.

Timelags of SideB

	1	2	3	4	5
1	0	-119			
2	1	0	-76		
3	1	1	0	93	
4	1	1	1	0	26
5	1	1	1	1	0

Peakstrengh of SideB

	1	2	3	4	5
1	0.7567	0.2387	0.1357	0.0786	0.0182
2	1	0.6387	0.3754	0.1621	-0.1075
3	1	1	0.5224	0.3629	0.0901
4	1	1	1	0.7124	0.4114
5	1	1	1	1	0.7368

Time-Peakstrengh of the Sides

	1	2	3	4	5
1	-804		-48	-1	
2	0.1785	-0.0094	-0.2381	-0.2143	0.0420

Timelags of SideA

	1	2	3	4	5
1	0	-120			
2	1	0	37		
3	1	1	0	47	
4	1	1	1	0	75
5	1	1	1	1	0

Peakstrengh of SideA

	1	2	3	4	5
1	0.7873	0.4749	0.1993	0.0037	-0.1331
2	1	0.6966	0.5432	0.2257	-0.0025
3	1	1	0.7092	0.4698	0.0332
4	1	1	1	0.7257	0.3961
5	1	1	1	1	0.7206

Figure B.3.2: The time lags are given for case 9 in these tables as well as the strength of the correlations for each thermistor pair.

Timelags of SideB

	1	2	3	4	5
1	0	-21			
2	1	0	-77		
3	1	1	0	73	
4	1	1	1	0	17
5	1	1	1	1	0

Peakstrengh of SideB

	1	2	3	4	5
1	0.8604	0.3891	0.0944	-0.0273	0.0344
2	1	0.8297	0.5790	0.2490	0.0325
3	1	1	0.8027	0.5432	0.1361
4	1	1	1	0.8438	0.4056
5	1	1	1	1	0.8677

Time-Peakstrengh of the Sides

	1	2	3	4	5
1			-12		
2	8.9658e-04	-0.1137	-0.2604	-0.0298	0.0548

Timelags of SideA

	1	2	3	4	5
1	0	-131			
2	1	0	6		
3	1	1	0	49	
4	1	1	1	0	28
5	1	1	1	1	0

Peakstrengh of SideA

	1	2	3	4	5
1	0.8002	0.4347	0.1395	-0.0033	-0.0698
2	1	0.8403	0.6011	0.2319	-0.0800
3	1	1	0.8163	0.4993	0.1106
4	1	1	1	0.8613	0.3767
5	1	1	1	1	0.8522

Figure B.3.3: The time lags are given for case 10 in these tables as well as the strength of the correlations for each thermistor pair.

Timelags of SideB

	1	2	3	4	5
1	0	-11			
2	1	0	-51		
3	1	1	0	81	
4	1	1	1	0	14
5	1	1	1	1	0

Peakstrengh of SideB

	1	2	3	4	5
1	0.8291	0.4462	0.2337	0.1468	0.0403
2	1	0.7441	0.5206	0.3809	0.1413
3	1	1	0.6988	0.4985	0.2351
4	1	1	1	0.7567	0.3518
5	1	1	1	1	0.8502

Time-Peakstrengh of the Sides

	1	2	3	4	5
1		86	-12	25	
2	-0.0138	-0.4331	-0.4391	-0.2970	0.0514

Timelags of SideA

	1	2	3	4	5
1	0				
2	1	0	10		
3	1	1	0	41	
4	1	1	1	0	18
5	1	1	1	1	0

Peakstrengh of SideA

	1	2	3	4	5
1	0.7391	0.0670	0.0108	0.0060	0.0324
2	1	0.6865	0.4663	0.1969	0.0260
3	1	1	0.6848	0.5114	0.1183
4	1	1	1	0.7475	0.4103
5	1	1	1	1	0.8409

Figure B.3.4: The time lags are given for case 11 in these tables as well as the strength of the correlations for each thermistor pair.

Timelags of SideB

	1	2	3	4	5
1	0	-5			
2	1	0	-34		
3	1	1	0	41	
4	1	1	1	0	3
5	1	1	1	1	0

Peakstrengh of SideB

	1	2	3	4	5
1	0.8468	0.2617	-0.0148	-0.0316	-0.0056
2	1	0.6811	0.3827	0.2506	0.0506
3	1	1	0.6397	0.5129	0.1889
4	1	1	1	0.7750	0.3943
5	1	1	1	1	0.8517

Time-Peakstrengh of the Sides

	1	2	3	4	5
1		47	1	29	4
2	-8.8189e-04	-0.2027	-0.3754	-0.3301	-0.1749

Timelags of SideA

	1	2	3	4	5
1	0	-56			
2	1	0	9		
3	1	1	0	15	
4	1	1	1	0	8
5	1	1	1	1	0

Peakstrengh of SideA

	1	2	3	4	5
1	0.8408	0.2912	0.0612	-0.0145	0.0017
2	1	0.7006	0.4345	0.2188	0.0417
3	1	1	0.6785	0.5050	0.1759
4	1	1	1	0.7167	0.3985
5	1	1	1	1	0.8170

Figure B.3.5: The time lags are given for case 12 in these tables as well as the strength of the correlations for each thermistor pair.

Timelags of SideB

	1	2	3	4	5
1	0	-13			
2	1	0	-48		
3	1	1	0	64	
4	1	1	1	0	7
5	1	1	1	1	0

Peakstrengh of SideB

	1	2	3	4	5
1	0.8663	0.5456	0.2031	0.0746	0.0656
2	1	0.8158	0.5609	0.3519	0.2294
3	1	1	0.8127	0.6306	0.4847
4	1	1	1	0.8010	0.5837
5	1	1	1	1	0.8184

Time-Peakstrengh of the Sides

	1	2	3	4	5
1		75	-3		
2	-0.0202	-0.4084	-0.2746	-0.0657	-0.0590

Timelags of SideA

	1	2	3	4	5
1	0	-109			
2	1	0	17		
3	1	1	0	41	
4	1	1	1	0	19
5	1	1	1	1	0

Peakstrengh of SideA

	1	2	3	4	5
1	0.8075	0.5419	0.3151	0.3225	0.2351
2	1	0.7433	0.6145	0.4910	0.2407
3	1	1	0.8113	0.6741	0.3604
4	1	1	1	0.8369	0.5379
5	1	1	1	1	0.7542

Figure B.3.6: The time lags are given for case 13 in these tables as well as the strength of the correlations for each thermistor pair.

References

[1] John Marshall and Friedrich Schott. Open-ocean convection: Observations, theory, and models. *Reviews of Geophysics*, 37(1):1–64, 1999.

[2] Paul H. Roberts and Eric M. King. On the genesis of the earth's magnetism. *Reports on Progress in Physics*, 76(9):096801, 2013.

[3] Chris A. Jones. Planetary magnetic fields and fluid dynamos. *Annual Review of Fluid Mechanics*, 43:583–614, 2011.

[4] Leon R. Glicksman. Energy efficiency in the built environment. *Physics Today*, 61(7):35, 2008.

[5] Frank P. Incropera. *Liquid cooling of electronic devices by single-phase convection*, volume 3. Wiley-Interscience, 1999.

[6] Alexander V. Getling. Rayleigh-Benard Convection; Structures and Dynamics. *Journal of Fluid Mechanics*, 382(1):374–378, 1999.

[7] Ernst L. Koschmieder. *Bénard cells and Taylor vortices*. Cambridge University Press, 1993.

[8] Eric M. King and Jonathan M. Aurnou. Thermal evidence for Taylor columns in turbulent rotating Rayleigh-Bénard convection. *Physical Review E*, 85:016313, Jan 2012.

[9] Francesca Chillà and Joerg Schumacher. New perspectives in turbulent rayleigh-bénard convection. *The European Physical Journal E*, 35(7):58, 2012.

[10] David Gubbins. The Rayleigh number for convection in the Earths core. *Physics of the Earth and Planetary Interiors*, 128(1-4):3–12, 2001.

[11] Gerald Schubert and Krista M. Soderlund. Planetary magnetic fields: Observations and models. *Physics of the Earth and Planetary Interiors*, 187(3-4):92–108, 2011.

[12] Eric M. King and Bruce A. Buffett. Flow speeds and length scales in geodynamo models: The role of viscosity. *Earth and Planetary Science Letters*, 371:156–162, 2013.

[13] Keith Julien, Antonio M. Rubio, Ian Grooms, and Edgar Knobloch. Statistical and physical balances in low Rossby number Rayleigh–Bénard convection. *Geophysical & Astrophysical Fluid Dynamics*, 106(4-5):392–428, 2012.

[14] Stephan Stellmach, Matthias Lischper, Keith Julien, Geoffrey Vasil, Jonathan S. Cheng, Adolfo Ribeiro, Eric M. King, and Jonathan M. Aurnou. Approaching the asymptotic regime of rapidly rotating convection: boundary layers versus interior dynamics. *Physical Review Letters*, 113(25):254501, 2014.

[15] Eyrian and Con-struct. convection cells— Wikimedia Commons, the free media repository, 2007. [Online; accessed 21-July-2018].

[16] Jonathan S. Cheng, Rudie P.J. Kunnen, Jonathan M. Arnou, and Keith Julien. A heuristic framework for extreme models of geostrophic convective turbulence. *Geophysical and Astrophysicl Fluid Dynamics*. (in review) arXiv:1703.02895.

[17] Richard J. A. M. Stevens, Herman J. H. Clercx, and Detlef Lohse. Heat transport and flow structure in rotating Rayleigh–Bénard convection. *European Journal of Mechanics-B/Fluids*, 40:41–49, 2013.

[18] Siegfried Grossmann and Detlef Lohse. Scaling in thermal convection: a unifying theory. *Journal of Fluid Mechanics*, 407:27–56, 2000.

[19] Willem V. R. Malkus. The heat transport and spectrum of thermal turbulence. *Proceedings of the Royal Society A*, 225:196, 1954.

[20] Guenter Ahlers, Siegfried Grossmann, and Detlef Lohse. Heat transfer and large scale dynamics in turbulent Rayleigh-Bénard convection. *Reviews of Modern Physics*, 81(2):503, 2009.

[21] Eric D. Siggia. High Rayleigh number convection. *Annual Review of Fluid Mechanics*, 26(1):137–168, 1994.

[22] Robert H. Kraichnan. Turbulent thermal convection at arbitrary Prandtl number. *The Physics of Fluids*, 5(11):1374–1389, 1962.

[23] Jonathan S. Cheng, Stephan Stellmach, Adolfo Ribeiro, Alexander Grannan, Eric M. King, and Jonathan M. Aurnou. Laboratory-numerical models of rapidly rotating convection in planetary cores. *Geophysical Journal International*, 201(1):1–17, 2015.

[24] Robert E. Ecke and Joseph J. Niemela. Heat transport in the geostrophic regime of rotating Rayleigh-Bénard convection. *Physical Review Letters*, 113(11):114301, 2014.

[25] Guenter Ahlers, Eric Brown, Francisco F. Araujo, Denis Funfschilling, Siegfried Grossmann, and Detlef Lohse. Non-Oberbeck–Boussinesq effects in strongly turbulent Rayleigh–Bénard convection. *Journal of Fluid Mechanics*, 569:409–445, 2006.

[26] Eric M. King, Stephan Stellmach, and Jonathan M. Aurnou. Heat transfer by rapidly rotating Rayleigh–Bénard convection. *Journal of Fluid Mechanics*, 691:568–582, 2012.

[27] Ronald N. Bracewell. *The Fourier transform and its applications*, volume 31999. McGraw-Hill New York, 1986.

[28] Thomas W. Körner. *Fourier analysis*. Cambridge university press, 1989.

[29] Peter Bloomfield. *Fourier analysis of time series: an introduction*. John Wiley & Sons, 2004.

[30] James S. Walker. *Fast Fourier transforms*. CRC press, 2017.

[31] Sophocles J. Orfanidis. *Optimum Signal Processing. An Introduction*. Graw-Hill Publishing Company, 1996.